UNIVERSIDAD NACIONAL AUTÓNOMA DE MEXICO

POSGRADO EN CIENCIA E INGENIERÍA DE MATERIALES
INSTITUTO DE INVESTIGACIONES EN MATERIALES

"A THEORETICAL STUDY OF SILICENE NANORIBBONS' ELECTRONIC STRUCTURE"

TESIS
QUE PARA OPTAR POR EL GRADO DE:
MAESTRO EN CIENCIA E INGENIERÍA DE MATERIALES

PRESENTA:
I.Q. HÉCTOR MANUEL LÓPEZ DE LA CERDA RÍOS

TUTOR PRINCIPAL

DR. SERGUEI FOMINE
INSTITUTO DE INVESTIGACIONES EN MATERIALES, UNAM

MIEMBROS DEL COMITÉ TUTOR

DR. TOMÁS ROCHA RINZA
INSTITUTO DE QUÍMICA, UNAM

DRA. MARÍA RENELA VALLADARES MC NELIS,
FACULTAD DE CIENCIAS, UNAM

CIUDAD DE MÉXICO, JUNIO, 2017

A Theoretical Study of Silicene Nanoribbons' Electronic Structure

by

I. Q. Héctor Manuel López de la Cerda Ríos

Submitted to the Graduate Program of Materials Science and Engineering
on March 14, 2017, in partial fulfillment of the
requirements for the degree of
Master of Science in Materials Science and Engineering

Abstract

In this thesis, we studied the electronic structure of silicene clusters with hydrogen passivated edges (H-SiNR) arranged in rectangular arrays parameterized by n_z and n_a, each denoting the length of the particular edges ubiquitous in every system. Where n_z and n_a are the number of non-nodal zig-zag sites and armchair bonds, respectively. We found that singlet spin multiplicity prevails in the H-SiNRs when $n_a<n_z$ but, surprisingly, transitions to a triplet multiplicity for certain structures with $n_a>n_z$. In both instances we end up with spin polarized zig-zag edge state materials with an antiferromagnetic arranging, with the exception between the two multiplicities being the type of coupling between these edges. A ferromagnetic and an antiferromagnetic type coupling between the zig-zag edge spin states corresponds to the triplet and singlet spin multiplicities, respectively. Interestingly, a ferromagnetic coupling would lead to spin specific transport along the zig-zag edges that may become useful for magnetic memory storage and quantum computers. Finally, as a means to give experimental researchers evidence for the detection of the relevant H-SiNRs, we calculated the Raman spectra for the ground states and found that the ratio of the G and D peak intensities may give indication whether the synthesized material is of singlet or triplet spin multiplicity.

Thesis Supervisor: Dr. Serguei Fomine
Title: Instituto de Investigaciones en Materiales, UNAM

Thesis Supervisor: Dr. Tomás Rocha Rinza
Title: Instituto de Química, UNAM

Thesis Supervisor: Dra. María Renela Valladares Mc Nelis
Title: Facultad de Ciencias, UNAM

Foreward

Here the intention is to notify the reader that this thesis is an extension of the article that was published by Serguei Fomine, Mildred S. Dresselhaus, Ricardo Pablo Pedro and I, that is referred here as [53]. The work reported in the latter article and of this thesis began with the desire to gain insight of silicene nanoribbons' electronic structure using a well defined methodology that has been at the foundation of the research done in our group but that has been enriched during my academic stay as well as through constructive discussions with Ricardo at his home institution. Therefore, all that is discussed and the way it is done is also present here in this thesis, in which some arguments have been expanded upon and some loose ends have been looked into. Ultimately, the reader may wish to read the article if in lack of time to read this thesis in it's entirety.

Acknowledgments

I would like to thank my mum, dad, sister, Ricardo Pablo Pedro, Mr. Salvador, and especially Dr. Serguei Fomine for giving me the opportunity to work with him, but also to be able to learn so much from him. Thank you all who have helped me and prodded me along this journey till the end.

Contents

List of Figures

List of Tables

Chapter 1

Introduction

1.1 Moore's Conundrum & Molecular Electronics

Since the conception of modern computers, scientists and engineers have been enthralled in ways of making them faster by adding evermore electronic components onto (micro)processors and so forth, accelerating the number of calculations and/or jobs the computer may execute with every new generation. There is even a name for it, it is called *Moore's Law*, which is named after the prediction made by Intel's co-founder Gordon E. Moore who stated that the number of components per integrated circuit would double annually [44], which later he revised it to happen every two years [45]. Until now this progression has been more or less upheld. However, the reason why this should interest us, producing ultrafast computers in general, is that it could help us make strides in scientific fields, such as artificial intelligence research projects, quantum chemistry, empowering research groups by enabling them to chose *ab initio* calculations that are normally constrained to systems composed of 1 to 20 atoms, and other physical sciences.

As a consequence of physical limitations, Moore's law can not go on *Ad Infinitum*. We are currently in an age whereupon dissipative phenomena will become an important factor in modelling silicon based circuit boards because of their saturation with transistors. Consequently, the spacing between them becomes so small that quantum phenomena such as tunnelling will need to be taken into account, thus making the

flow of electric current less efficient throughout the circuit board. Seemingly, one way of overcoming this is by theorizing nano-scaled systems that have electronic properties which resemble macroscopic electronic components, such as wires, transistors, diodes, semiconductors, etc. This branch of research is called *Molecular Electronics*, and up until now has been focused on one-dimensional (1D) systems, in part, due to their relative ease to synthesize and to perform calculations with higher-end quantum chemical methods that include more than one configuration. But with the advent of the modern computer and density functional theory (DFT), as well as the progress made in surface chemistry, two-dimensional (2D) systems have recently gained momentum in the scientific community across the world [6, 66, 9]. Their accessibility prodded on by the technological advancements mentioned in the last sentence. Moreover, modern approximations to studying their electronic structure like DFT have helped by predicting and understanding newfound materials, alerting the experimental community of scientists to hone in on relevant systems and vice versa.

1.2 Graphene & 2D Crystals

In 2004, a highly interesting 2D crystal that was once thought as an 'academic' material was obtained through mechanical exfoliation of graphite. It is known as graphene and is basically a monolayer composed of conjugated sp^2 carbon atoms which form a honeycomb lattice [51]. Graphene is the building block of many forms of carbon systems such as carbon nanotubes, and fullerenes as shown in Fig. 1-1. In general, 2D crystals were thought to be non-existent because of thermodynamic instabilities associated to thermal fluctuations that would provoke atomic displacements comparable to their interatomic distances at any finite temperature [55, 31]. Nevertheless, the existence of graphene may be explained due to its extraction from a 3D material, quenching it in a metastable state. Also, its small scale and strong bonds prevent thermal fluctuations from generating crystal defects even at high temperatures [42].

Furthermore, graphene's electronic properties have been studied and found to have ballistic charge transport with a pronounced ambipolar electric field effect (Fig. 1-2).

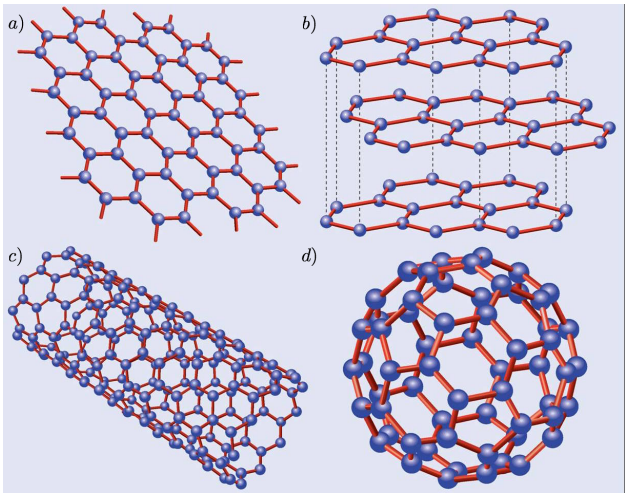

Figure 1-1: Allotropes of carbon built from (a) graphene are (b) graphite, (c) carbon nanotubes, and (d) fullerene [55].

This means, it has been observed that because it's an zero-gap semiconductor (semimetal), the amount of its charge carriers, be it electrons or holes, may be tuned by exposure of a gate voltage in concentrations as high as 10^{13} cm^{-2} and their mobilities can exceed 15,000 cm^{2}V^{-1}s^{-1} even under ambient conditions [51, 52, 50]. These values are much higher than any typical semiconductor in use today, see Table 1.1. Graphene's unusual properties are explained using the tight binding approach, after which it was discovered that their electrons act like massless Dirac fermions around the Dirac points, with a Fermi velocity (v_F) of about $\frac{3}{1000}c$. A visual aid of the latest statement can be seen in Figure 1-3, in which the linear electron dispersion that conforms the Dirac point is described by the Dirac equation for particles with zero mass and with the Fermi velocity of the particle substituting the speed of light. The linear energy dispersion is given by $\pm v_F \hbar k$, where k is the Bloch wave vector.

Table 1.1: Electronic properties for bulk materials [46] and graphene [5] at 300 K.

Property	Si	Ge	GaAs	Graphene on SiO_2 substrate
Electron Mobility [cm^{2}V^{-1}s^{-1}]	1,417	3,900	8,800	40,000
Hole Mobility [cm^{2}V^{-1}s^{-1}]	471	1,900	400	40,000
Carrier Concentration	1.45x10^{10} cm^{-3}	2.4x10^{13} cm^{-3}	1.79x10^6 cm^{-3}	10^{12} cm^{-2}

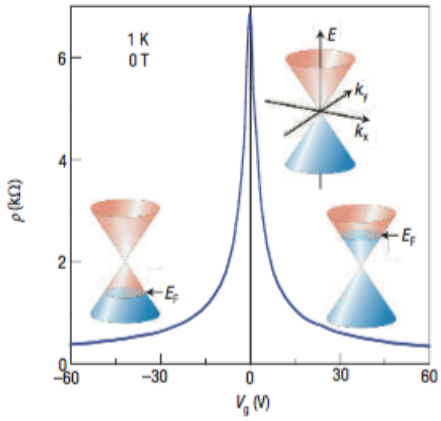

Figure 1-2: Ambipolar electric field effect in a graphene monolayer. The accompanying images indicate the changes made in graphene's band structure by varying the gate voltage (V_g) and relating it to its resistivity ρ indicating an increase of charge carriers with its exposure to an electrical potential.

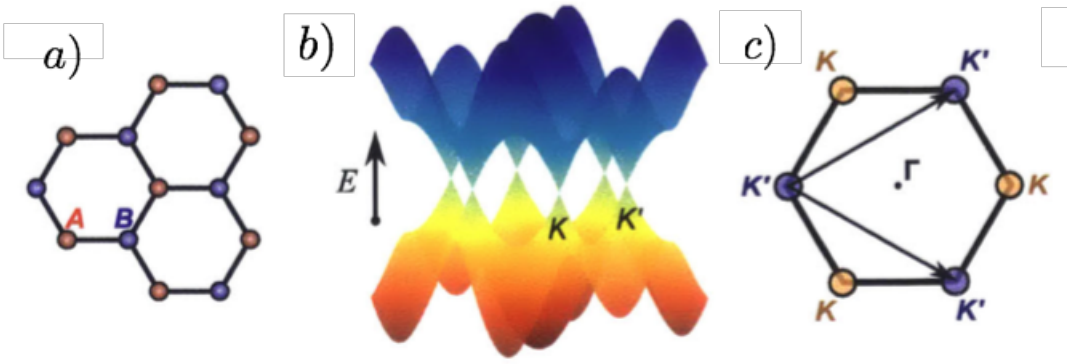

Figure 1-3: Graphene's electronic structure as obtained using tight binding. a) Graphene is composed of two sublattices, A and B. b) Its band structure is comprised of two inequivalent Dirac points, K and K', where the conduction and valence bands meet. K and K' are different due to the sublattices, A and B. c) The inequivalent Dirac points meet at the edges of the first Brillouin zone.

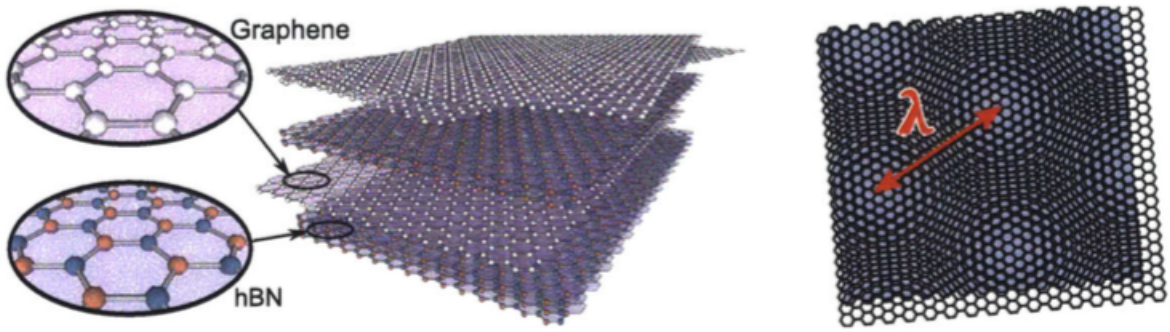

Figure 1-4: Example of a stacked van der Waals heterostructure comprised of graphene and hexagonal boron nitride monolayers, imperfectly layered so that they form Moiré patterns.

As attractive as graphene's properties may be for the electronic industry, its most apparent drawback is its lack of an intrinsic energy gap between the occupied π states and π^* states, making it impossible for its inclusion in the construction of electronic logic components. Thus, interest has poured over to other 2D monolayer crystals, some known as van der Waals materials, which may also be mechanically exfoliated from their bulk counterparts and whose electronic properties are also modelled by massless Dirac fermions. Examples of layered van der Waals materials are graphene, hexagonal boron nitride (hBN) and transition metal dichalcogenides (TMD). Additionally, the previously mentioned materials may also be stacked accordingly to produce heterogeneous van der Waals structures, customizing its electronic properties as a function of the type and number of layers, as well as, their relative phase to each other (Fig. 1-4). Other low dimensional materials may be obtained through chemical vapour deposition (CVD) and/or epitaxy growth upon specific substrates, usually metals. For example, the remaining of group IV elemental materials, silicene, germanene and stanene. From these, silicene is considered of greatest interest due to silicon's role in the fabrication of current electronic components, hence a breakthrough in computation capabilities may be just around the corner if the current Si based microporcessors' production lines can be adapted to incorporate silicene into their workings. Thus, knowledge of silicon's 2D analogue electronic properties is of both fundamental and applied interest.

1.3 Silicene

Although silicene was first theoretically predicted to be stable in nature by using first-principles calculations such as density functional theory (DFT) and the tight-binding model [72, 2], it was not until the actual synthesis of silicene [65, 54, 14] that the intense research of this material started due to its similarities with graphene. Silicene is composed of Si atoms with a honeycomb structure like graphene, but with a buckled hexagonal layered structure composed of two sublattices which are on different planes (Fig. 1-5). As in graphene, the valence and conduction bands of silicene meet at two inequivalent Dirac points (K and K' points) at the Fermi level [2]. This peculiar band structure gives rise to exceptionally high electrical and thermal conductivities [80] similar to those of graphene, and also to many other interesting properties, such as a quantum spin Hall effect due to its additional spin-orbit coupling [37] compared to graphene. However, in spite of there existing already conclusive experimental evidence for silicene formation upon different types of substrates [11, 14, 62], the inherent difficulty of its synthesis has imposed constraints in obtaining free-standing silicene. Consequently, hindering the understanding of the influences of doping, external fields, defects, and magnetic moments on the properties of this material, limiting silicene's exploitation in nanoelectronics and high-efficiency thermoelectric materials [25, 73, 80]. Another roadblock from preventing further study of silicene is the fact that it is highly reactive under normal atmospheric conditions. Where the $sp^2 - sp^3$ bonds in silicene break to form bonds with O_2 in the environment, thereby, providing it necessary to find non-reactive encapsulation materials and methods for silicene to be probed experimentally. Although, possible solutions have been reported in the following references [74, 43], encapsulation of the silicene was done with aluminum (III) oxide, and a field effect transistor was later produced with such technics [74], detecting a carrier mobility $\sim$10 $cm^2V^{-1}s^{-1}$ in their devices. The latter low carrier mobility probably resulting from the coupling of strong out-of-plane acoustic (ZA) phonons, due to silicene's intrinsic buckled structure, with its substrate.

Currently, most of the research on silicene has been done using theoretical and

computational approaches, such as tight-binding models [20], density functional theory (DFT) [19], and diffusion quantum Monte Carlo (DQMC) calculations [17, 77]. Such approaches have indeed resulted in a better understanding of the effects of relatively high spin-orbit coupling [38], increased interlayer binding energy in layered materials, the presence of the quantum spin Hall effect [37], and the possibility of exploring topological phases of silicene under an external field perpendicular to the silicene layers [49]. However, most of the theoretical findings reported for silicene have been done using an inadequate DFT level of theory with the generalized gradient approximation (GGA) functionals, local density approximation (LDA) functionals, and plane waves bases, none of which fully account for electron correlations. Therefore, only calculational approaches that are based on multireference wave functions are capable of predicting the peculiarities of the silicene electronic behavior, such as in large conjugated systems which potentially possess multi-configurational ground states [30, 61, 76]. Thus, the most used method to at least treat static correlation is known as a complete active space self-consistent field (CASSCF) approach[64]. But the CASSCF method is limited by the size of the system due to the huge number of available configurations that can be generated in the active space of the system. The latter issue is why using single-determinant approaches with an unrestricted formalism for the wave function construction turn out to be an alternative approach that is useful for large systems.

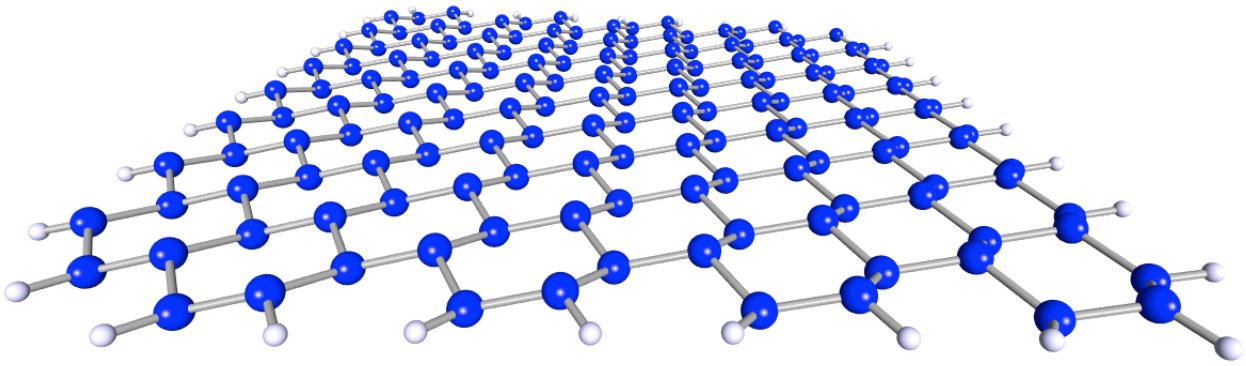

Figure 1-5: A view of silicene (blue atoms) with hydrogen passivated edges (white atoms).

The application of single-determinant methods along with an unrestricted formalism for the wave function allows us to study systems with $\langle S^2 \rangle \geq 0$, but the results are often qualitatively poor, and the wave function is no longer an eigenfunction of the spin operator $\hat{S}^2$. Therefore the solutions thus obtained are spin-mixed, which is also known as spin-contamination. In many cases the spin contamination from higher spin states is quite negligible [67] but for systems with unpaired electrons, such as graphene and silicene, the spin contamination could be quite significant [23]. Hence, we wished to study silicene's electronic properties in a systematic manner to probe its multiconfigurational character and to determine its multiplicity in the ground state, because systems with $S = 1$ can be potentially applied to spintronics [36]. Consequently, the problem of determining whether or not silicene possesses a multiconfigurational character and how to address electron correlation within this material should be considered. Thus, the goal of this thesis is to explore the previously stated observations of the ground state's multiplicity and give additional insight to silicon's 2D structures, i.e. analysis of the Raman spectra for relevant sizes with the objective in mind of aiding experimenters that wish to explore our results by synthezising these systems.

The following chapter considers the theoretical background underlying this thesis.

Chapter 2

Electronic Structure

Since the conception of quantum mechanics by Erwin Schrödinger and Werner Heisenberg in the 1920's, leading theorists have pushed the limits of its groundwork to an unimaginable series of systems. In the context of this work, we will focus only on solutions and simplifications of Schrödinger's time independent equation 2.1 (SE), applied to non-relativistic many body systems.

$$\hat{\mathrm{H}}\,\psi\left(\mathbf{r}_1,\mathbf{r}_2,\ldots\mathbf{r}_N,\mathbf{R}_1,\mathbf{R}_2,\ldots\mathbf{R}_M\right)=\mathrm{E}\,\psi\left(\mathbf{r}_1,\mathbf{r}_2,\ldots\mathbf{r}_N,\mathbf{R}_1,\mathbf{R}_2,\ldots\mathbf{R}_M\right), \tag{2.1}$$

where $\mathbf{r}_i$ and $\mathbf{R}_k$ are the spatial coordinates for the i-th electron and k-th nucleus, respectively, and E is the energy of the system with N electrons and M nuclei that is described by the Hamiltonian, $\hat{\mathrm{H}}$. For most molecules, the following hamiltonian is sufficient for their study, in which we have used atomic units to simplify notation.

$$\begin{aligned}\hat{\mathrm{H}} &= -\frac{1}{2}\sum_{i}^{N}\nabla_i^2-\frac{1}{2}\sum_{a}^{M}\frac{1}{\mathrm{M}_a}\nabla_i^2+\sum_{j<i}^{N}\frac{1}{|\mathbf{r}_i-\mathbf{r}_j|}-\sum_{a,i}^{M}\frac{\mathrm{Z}_a}{|\mathbf{r}_i-\mathbf{R}_a|}+\sum_{b<a}^{M}\frac{\mathrm{Z}_a\mathrm{Z}_b}{|\mathbf{R}_a-\mathbf{R}_b|}\\ &= \hat{\mathrm{T}}_e+\hat{\mathrm{T}}_{nuc}+\hat{\mathrm{V}}_{e,e}+\hat{\mathrm{V}}_{ext}+\hat{\mathrm{V}}_{nuc,nuc}\end{aligned} \tag{2.2}$$

Here, M_a is the mass of nucleus a and Z_a is the atomic number of the same nucleus. Also, $\hat{\mathrm{T}}_e$ and $\hat{\mathrm{T}}_{nuc}$ are respectively the electron and nuclei kinetic operators, whereas, $\hat{\mathrm{V}}_{e,e}$, $\hat{\mathrm{V}}_{e,nuc}$, and $\hat{\mathrm{V}}_{nuc,nuc}$ stand for the electron-electron repulsion, the electron-nucleus

attraction, and the repulsion between nuclei, respectively.

Using 2.1 and solving for ψ by plugging in the above hamiltonian 2.2, would let us obtain all the system's information in the form of the wave function. The only thing left to do, would be to squeeze out its contents through operations concerning the appropriate hermitian operators. However, the non relativistic time independent Schrödinger equation almost never be solved analytically, especially for molecules that are made up of more than two atoms. This limitation is due to the coupling of various coordinates of the different bodies that conform the molecule, making it impossible to separate them during integration. Thus, we try to find acceptable approximations that would make the equations easier to solve.

One approximation consists of splitting the wave function into two parts, one of which contains all there is to know about the electrons and the other about the nuclei, 2.3. The separation of these coordinate spaces is a product of the Born-Oppenheimer approximation, principally justified by how greater the mass of the proton is that of the electron's. This is the subject of the next section.

$$\psi\left(\mathbf{r}_1, \mathbf{r}_2, \ldots \mathbf{r}_N, \mathbf{R}_1, \mathbf{R}_2, \ldots \mathbf{R}_M\right) = \phi_{elec}\left(\mathbf{r}_1, \mathbf{r}_2, \ldots \mathbf{r}_N; \mathbf{R}_1, \mathbf{R}_2, \ldots \mathbf{R}_M\right) \phi_{nuc}\left(\mathbf{R}_1, \mathbf{R}_2, \ldots \mathbf{R}_M\right) \tag{2.3}$$

Additionally, for more reference and follow through on most of this chapter's content, please revise the following references of great books, [24, 71, 28], which served as great influence for most of this chapter's content.

2.1 The Born–Oppenheimer Approximation

As already mentioned, the Born–Oppenheimer approximation consists of applying the separation of variables method to the original wave function ψ. Dividing it into parts that individually describe phenomena attributed to the electrons and nulcei. This is generally a good approximation because the smallest nucleus, a proton, is about 2,000 times heavier than the electron. So it can be considered, as a first approximation, that the electrons move in a field of fixed protons. Therefore, parts

of the hamiltonian containing information of the nuclei become parameters fixed by the unchanging nuclei coordinates. So forth, $\hat{\mathrm{V}}_{nuc,nuc}$ becomes a fixed value and any constant summed to an eigenvalue problem makes no difference. Hence, we are only left with following hamiltonian,

$$\hat{\mathrm{H}}_{elec} = -\frac{1}{2}\sum_{i}^{N}\nabla_i^2 + \sum_{j<i}^{N}\frac{1}{|\mathbf{r}_i - \mathbf{r}_j|} - \sum_{a,i}^{M}\frac{\mathrm{Z}_a}{|\mathbf{r}_i - \mathbf{R}_a|}, \tag{2.4}$$

in which, the remaining terms describe only the motion of N electrons in a field of M nuclei. That is why it is called the electronic hamiltonian, $\hat{\mathrm{H}}_{elec}$. Necessarily, equation 2.1 must also change, albeit subtly, to reflect the fact that we are only dealing with the electrons,

$$\hat{\mathrm{H}}_{elec}\,\phi_{elec} = \mathrm{E}_{elec}\,\phi_{elec} \tag{2.5}$$

Wherein $\phi_{elec} = \phi(\mathbf{r}_1, \mathbf{r}_2, \ldots, \mathbf{r}_N; \mathbf{R}_1, \mathbf{R}_2, \ldots \mathbf{R}_M)$, i.e. the electronic wave function is implicitly dependent on the nuclear coordinates as a parameter. This is what is meant with the $(\mathbf{r}_1, \mathbf{r}_2, \ldots, \mathbf{r}_N; \mathbf{R}_1, \mathbf{R}_2, \ldots, \mathbf{R}_M)$ notation. As a result, the electronic energy, E_{elec} is also parametrically dependent on the nuclear coordinates, and the total energy is given by

$$\mathrm{E}_{tot} = \mathrm{E}_{elec}\,(\mathbf{R}_1, \mathbf{R}_2, \ldots, \mathbf{R}_M) + \sum_{b<a}^{M}\frac{\mathrm{Z}_a\mathrm{Z}_b}{|\mathbf{R}_a - \mathbf{R}_b|}. \tag{2.6}$$

The electronic structure of a system of many bodies, in the case of this study, silicene nanoribbons, could be described by solving equations 2.5 and 2.6. Their solutions would give us an approximation to the ground state energy and its respective electronic wave function by variation of two parameters, albeit separately, nuclear coordinates and the atomic functions' coefficients. The latter is a consequence of the variational principle. It should be emphasized that the total energy, E_{tot}, lacks any contribution of the nuclear kinetic energy, which can only be added by using the nuclear wave function.

Upon completing this task, the nuclear wave function can now be obtained by

considering that a sufficient approximation to its Hamiltonian is taking the expected value of the electronic Hamiltonian and summing the remaining nuclear contributions. The fact that the electrons are moving at much higher speeds than the nuclei, makes it reasonable to take their average and sum their value to the remaining terms, to obtain.

$$\begin{aligned}\hat{H}_{nuc} &= -\frac{1}{2}\sum_{a}^{M}\frac{1}{M_a}\nabla_i^2 + \mathrm{E}_{elec}\left(\mathbf{R}_1, \mathbf{R}_2, \ldots, \mathbf{R}_M\right) + \sum_{b<a}^{M}\frac{Z_a Z_b}{|\mathbf{R}_a - \mathbf{R}_b|} \\ &= -\frac{1}{2}\sum_{a}^{M}\frac{1}{M_a}\nabla_i^2 + \mathrm{E}_{tot}\end{aligned} \tag{2.7}$$

Additionally,

$$\begin{aligned}&\hat{H}_{nuc}\,\phi_{nuc} = \mathrm{E}_{BO}\,\phi_{nuc}, \\ &\phi_{nuc} = \phi\left(\mathbf{R}_1, \mathbf{R}_2, \ldots \mathbf{R}_M\right).\end{aligned} \tag{2.8}$$

In which E_{BO} is the Born–Oppenheimer approximate of the energy in equation 2.1. Using equations 2.7 and 2.8, one can obtain the vibrational, rotational and translational energies of a molecule. Hence, giving us the possibility to calculate the infrared (IR) and Raman spectra of any molecule that can be approximated with these considerations. Thus cation must be exercised when these approximations are expected or known to fail; when two electronic states are almost degenerate, and in processes where the molecule is greatly photoexcited[1].

2.2 The Hartree-Fock Method

The Born–Oppenheimer approximation is fundamental to all of quantum chemistry, for it is the bedrock of all first principles calculations. Now what is left is to find acceptable wave functions for both electrons and nuclei, to which we can start looking for by using the fact that we are dealing with fermions. This implies, their wave

[1]Because we will only deal with the electronic aspect of equation 2.1, we will drop the *elec* labels of equation 2.5 and only specify when we are dealing with Hamiltonians different than the electronic one.

functions must be antisymmetric with respect to interchanging spatial and spin coordinates of a pair of them. These coordinates are the spatial and spin labels that describe an electron in a specific system. The spin label acts as a means of marking an electron with either up, $\alpha(s)$, or down, $\beta(s)$ spin. The variable s representing the spin of an electron.

The first approximation was done by using determinants of matrices whose components were single electron spin orbitals, $\chi(\mathbf{x})$, i.e. a function that describes an electrons' spatial and spin orientation 2.9.

$$\chi(\mathbf{x}) = \phi(\mathbf{r})\,\sigma(s)\,, \quad \sigma(s) = \{\alpha(s), \beta(s)\} \tag{2.9}$$

These antisymmetric entities are called Slater determinants, Φ_{SD},

$$\phi \approx \Phi_{SD} = \frac{1}{\sqrt{\mathrm{N}!}}\mathrm{Det}\left(\chi_1(\mathbf{x}_1)\ \chi_2(\mathbf{x}_2)\cdots\chi_{\mathrm{N}}(\mathbf{x}_{\mathrm{N}})\right). \tag{2.10}$$

Orthonormality of the spin orbitals is also maintained, thus, becoming a constraint for the selection of the set of admissible functions. Moreover, the Slater determinant is an approximation to the electronic wave function, ϕ_{elec}, now that it considers a set of non-interacting but spin correlated electrons as the many body wave function, with the necessary antisymmetric property. Upon following this consideration, we explore the expectation value of the electronic hamiltonian with N electrons and M nuclei.

$$\begin{aligned}
\mathrm{E}_{HF} &= \int \Phi_{SD}^{\dagger}\ \hat{\mathrm{H}}\ \Phi_{SD}\,\mathrm{d}\mathbf{x}_1\,\mathrm{d}\mathbf{x}_2\ldots\mathrm{d}\mathbf{x}_{\mathrm{N}} \\
&= \sum_{i}^{\mathrm{N}}\int \chi_i^*(\mathbf{x}_1)\left(-\frac{1}{2}\nabla_i^2 - \sum_{a}^{\mathrm{M}}\frac{\mathrm{Z}_a}{|\mathbf{r}_1-\mathbf{R}_a|}\right)\chi_i(\mathbf{x}_1)\,\mathrm{d}\mathbf{x}_1 \\
&+ \frac{1}{2}\sum_{i,j}^{\mathrm{N}}\iint\left(|\chi_i^*(\mathbf{x}_1)|^2\,\frac{1}{|\mathbf{r}_1-\mathbf{r}_2|}\,|\chi_j(\mathbf{x}_2)|^2 - \chi_i^*(\mathbf{x}_1)\chi_j^*(\mathbf{x}_2)\frac{1}{|\mathbf{r}_1-\mathbf{r}_2|}\chi_j(\mathbf{x}_1)\chi_i(\mathbf{x}_2)\right)\mathrm{d}\mathbf{x}_1\,\mathrm{d}\mathbf{x}_2 \\
&= \sum_{i}^{\mathrm{N}}\int \mathrm{h}_i\,\mathrm{d}\mathbf{x}_1 + \frac{1}{2}\sum_{i,j}^{\mathrm{N}}\iint(\mathrm{J}_{ij}-\mathrm{K}_{ij})\,\mathrm{d}\mathbf{x}_1\,\mathrm{d}\mathbf{x}_2
\end{aligned} \tag{2.11}$$

The expectation value of the Hamiltonian is made up of one- and two- particle integrals which are given by h_i, J_{ij}, and K_{ij}. The one-particle integral, $h_i(\mathbf{x}_1)$, contains the electronic kinetic energy, as well as its interaction with all nuclei. On the other hand, J_{ij} is the Coulombic repulsion expression between two electrons described by χ_i and χ_j, while K_{ij} is the exchange operator, which does not have a classical analogue. The latter energy contribution arises from the fact that electrons are identical particles, consequently, limiting our knowledge on which electron is exactly where and is in which spin orbital. But there is a constraint for participating exchange electrons, the electrons of the same spin are the only ones that contribute to $K_{ij}(\mathbf{x}_1, \mathbf{x}_2)$ because of the orthogonality of the spin functions and the fact that the exchange operator does not depend on the spin coordinates. Moreover, this term stabilizes the electron repulsion, in part contributing to lowering the energy upon the bonding of different species, making it essential for the understanding of chemical bonding. The exchange contribution is thus a consequence of the asymmetry of the wave functions for fermions and a lasting reminder of Pauli's wonderful but mysterious principle. It should also be emphasized, the possibility of artificial contributions of the two-particle integrals known as self-interaction upon practice of the method. This is brought on by the fact that we are summing with respect to the spin orbitals and not electrons, the term $i = j$ is possible and non-zero, which can be troublesome with other calculation methods. But in the case of the Hartree-Fock (HF) approximation, $J_{ij}(\mathbf{x}_1, \mathbf{x}_2)$ and $K_{ij}(\mathbf{x}_1, \mathbf{x}_2)$ cancel themselves out when $i = j$.

Additionally, the $J_{ij}(\mathbf{x}_1, \mathbf{x}_2)$ and $K_{ij}(\mathbf{x}_1, \mathbf{x}_2)$ integrals are reduced to mean field functions by approximating that each electron interacts with a field created by all other electrons which are also assumed to be static, thus, simplifying the the N-1 interactions an electron experiences to just a pairwise one. The equations are of the following form:

$$\begin{aligned} \hat{J}_j\, \chi_i(\mathbf{x}_1) &= \int |\chi_j(\mathbf{x}_2)|^2 \frac{1}{|\mathbf{r}_1 - \mathbf{r}_2|} \mathrm{d}\mathbf{x}_2 \chi_i(\mathbf{x}_1), \\ \hat{K}_j\, \chi_i(\mathbf{x}_1) &= \int \chi_j(\mathbf{x}_2)^* \frac{1}{|\mathbf{r}_1 - \mathbf{r}_2|} \chi_i(\mathbf{x}_2) \mathrm{d}\mathbf{x}_2 \chi_j(\mathbf{x}_1). \end{aligned} \tag{2.12}$$

It can be observed that the weighted value of the approximated Coulomb repulsion is of local character, for its value is entirely dependent on the value of $\chi_i(\mathbf{x}_1)$, as opposed to $\hat{\mathrm{K}}_j\,\chi_i(\mathbf{x}_1)$ which depends on the value of χ_i in all $\mathbf{x}_2$ space.

Furthermore, the minimization of the HF energy, E_{HF}, from equation 2.11 is done by varying the spin orbitals, along with considering the constraint that the spin orbitals remain orthonormal. This originates the HF equations, including the introduction of the orbital energies, ϵ_i, as lagrangian multipliers.

$$\begin{aligned} \hat{f}_i\,\chi_i &= \epsilon_i\,\chi_i,\ i = 1, 2, \ldots, N. \\ \hat{f}_i &= -\frac{1}{2}\nabla_i^2 - \sum_a^{\mathrm{M}} \frac{\mathrm{Z}_a}{|\mathbf{r}_i - \mathbf{R}_a|} + \mathrm{V}_a \end{aligned} \tag{2.13}$$

The Fock operator, $\hat{f}$, contains all relevant information for the calculation of the approximated orbital energies, while being an effective one-electron operator. Meanwhile, the HF potential, V_{HF}, contains the simplified versions of the two-electron repulsion operators, $\hat{\mathrm{J}}_j$, and $\hat{\mathrm{K}}_j(\mathbf{x}_1)$,

$$\mathrm{V}_{HF}(\mathbf{x}_1) = \sum_j^{\mathrm{N}} \left(\hat{\mathrm{J}}_j(\mathbf{x}_1) - \hat{\mathrm{K}}_j(\mathbf{x}_1) \right). \tag{2.14}$$

Thus, the above equations average the repulsive potential experienced by the i-th electron due to the remaining $N-1$ electrons. Consequently overestimating one of the aspects of the hamiltonian, the Coulombic electron repulsion. A way to improve our results would be by inserting what is called electron correlation in which the shortcomings of the HF method are taken into account, such as the instantaneous repulsion of the electrons, dynamical correlation, and the fact that the ground state of the molecule is not always well described by one Slater determinant but by other configurations, which include excited ones, static correlation.

$$\mathrm{E}_C^{HF} = \mathrm{E}_0 - \mathrm{E}_{HF} \tag{2.15}$$

Although, the HF method gives us the energetically best single Slater determinant

with the provided spin orbitals, it is still not enough to give the real ground state energy, E_0. The error of the calculated energy given by the difference of the true interacting system with the HF energy is called the correlation energy and given by equation 2.15. A solution for static correlation would be the implementation of more Slater determinants that represent the excited states of the system by replacing a column of the HF function by a virtual orbital. This method of calculation is called configuration interaction (CI) and will be addressed in the following sections.

2.3 Density Functional Theory

Density functional theory (DFT) has been highly exploited in the past twenty years due to its versatility to tackle all sort of physical systems, including solids, biological processes, and more. Its flexibility is achieved from using the electron density, $\rho(\mathbf{r})$, which is a function of only 3 variables, unlike the $4N$ variables that represent the spatial and spin coordinates of N electrons for the wave function (without considering the electrons' spin).

$$\begin{aligned} \rho(\mathbf{r}) &= \int \cdots \int \psi(\mathbf{x}, \mathbf{x}_2, \ldots, \mathbf{x}_\mathrm{N})^* \psi(\mathbf{x}, \mathbf{x}_2, \ldots, \mathbf{x}_\mathrm{N}) \, \mathrm{d}s \, \mathrm{d}\mathbf{x}_2 \ldots \mathrm{d}\mathbf{x}_\mathrm{N} \\ \mathrm{N} &= \int \rho(\mathbf{r}) \, \mathrm{d}\mathbf{r} \end{aligned} \tag{2.16}$$

This highly reduces the amount of computation for the calculation of the ground state function, although $\hat{\mathrm{V}}_{e,e}$ is still to be considered. Eventually, the latter is approximated by a combination of physical considerations that provide quantitively good results, but improvements are still much needed to find a universal exchange-correlation functional capable of correctly treating any type of molecular system. Still, DFT comes from an exact formulation and must not be confused as being a semi-empirical method for its foundations are rigorously proven; although in practice, it may very well be!

Ultimately, DFT may be seen as a reformulation of quantum mechanics, with the electron density, $\rho(\mathbf{r})$, replacing the coveted wave function, $\psi(\mathbf{r})$, obtained from equation 2.1. But as can be seen in the following diagrams, both equation are connected

in an intimate manner, as one can be obtained from the other.

$$\mathrm{V}_{ext}(\mathbf{r}) \overset{SE}{\Longrightarrow} \psi(\mathbf{x}, \mathbf{x}_2, \ldots, \mathbf{x}_\mathrm{N}) \overset{\langle A \rangle_\psi}{\dashrightarrow} \text{observables.} \tag{2.17}$$

Whereas, the DFT formulation is somewhat reversed.

$$\rho(\mathbf{r}) \Rightarrow \mathrm{V}_{ext}(\mathbf{r}) \Rightarrow \hat{\mathrm{H}} \Rightarrow \psi(\mathbf{x}, \mathbf{x}_2, \ldots, \mathbf{x}_\mathrm{N}) \tag{2.18}$$

The above procedure was first rigorously established by Hohenberg and Kohn (HK) in 1964 [22], both of which are DFT's founding fathers, and whose theorems will be further discussed in subsequent sections.

Before moving on, we wish to give a rather non rigorous definition of what a functional is, especially now that we're dealing with a theory that extensively uses them. A functional is nothing more than a transformation that goes from a function to a scalar. For example, a defined integral is a functional for any well defined function in the (a, b) interval, like $F[f(x)] = \int_a^b f(x)\,\mathrm{d}x$, since it connects the function f(x) in the interval (a,b) to a scalar. Where the usual notation of a functional is determined much like a function but with the dependent function variable in square brackets, as written in the past example. Thus it can be observed, having knowledge of the variational principle in quantum mechanics, that the energy of a molecular system is a functional of the wave function, E[ψ].

2.3.1 Hohenberg–Kohn Theorem

In 1964, an article written by HK [22] laid the foundations of DFT, by proving in a rigorous manner the possibility of replacing the wave function with the electron density. Therein, it is proven that the ground state electron density contains all of the system's information and it is constructed by anti-symmetric wave functions. Moreover, the article proves the following two theorems about $\rho(\mathbf{r})$ and its relation to the energy functional, expectation value of the Hamiltonian, and to Schrödinger's ground state wave function for non degenerate systems. Although, M. Levy [34] and

E. Lieb [35] afterwards, independently, generalized the HK theorems to degenerate systems.

1st HK theorem: For any system of interacting particles in an external potential $\mathrm{V}_{ext}(\mathbf{r})$, the ground state density, ρ_0, can also determine the potential up to an additive constant. As a consequence, ρ_0 not only determines ψ_0 but also the Hamiltonian and thus, all excited states, $\psi_k(\mathbf{x}_1, \mathbf{x}_2, \ldots, \mathbf{x}_\mathrm{N}) = \psi_k[\rho_0]$ The ground state many body wave function $\psi_0(\mathbf{x}_1, \mathbf{x}_2, \ldots, \mathbf{x}_\mathrm{N})$ is a functional of the ground state electron density $\rho_0(\mathbf{r})$.

$$\psi_0(\mathbf{x}_1, \mathbf{x}_2, \ldots, \mathbf{x}_\mathrm{N}) = \psi_0[\rho_0(\mathbf{r})] \tag{2.19}$$

But any observable, $O = \left\langle \hat{O} \right\rangle$, is a functional of $\psi_0(\mathbf{x}_1, \mathbf{x}_2, \ldots, \mathbf{x}_\mathrm{N})$, thus $O[\psi_0(\mathbf{x}_1, \mathbf{x}_2, \ldots, \mathbf{x}_\mathrm{N})] = O[\rho_0(\mathbf{r})]$.

2nd HK theorem: Now that any observable can be obtained using the electron density, including the molecular energy, the variational principle still holds, but now is done by minimizing the energy functional by varying $\rho_0(\mathbf{r})$,

$$\begin{aligned} \mathrm{E}_0 &= \mathrm{E}[\rho_0(\mathbf{r})] \leq \mathrm{E}[\rho(\mathbf{r})] \\ \mathrm{E}[\rho(\mathbf{r})] &= \min_{\psi \to \rho} (\mathrm{T} + \mathrm{V}_{e,e} + \mathrm{V}_{ext}) \end{aligned} \tag{2.20}$$

So, if the energy is evaluated with a electron density different from the ground state one, the energy would be greater than E_0. Therefore, these two theorems give us the necessary rigour to change from the wave function to the electron density, for the electron density is unique for each $\hat{V}_{ext}$, and minimizes the energy. Additionally, the energy functional is also given as

$$\begin{aligned} \mathrm{E}[\rho(\mathbf{r})] &= \min_{\psi \to \rho} (T + V_{ext} + V_{e,e}) \\ &= \mathrm{T}[\rho] + \mathrm{V}_{e,e}[\rho] + \mathrm{V}_{ext}[\rho] = \mathrm{F}[\rho] + \mathrm{V}_{ext}[\rho] \end{aligned} \tag{2.21}$$

In which $T[\rho]$ and $V_{e,e}[\rho]$ are the universal operators for they are always the same for any molecular Hamiltonian, whereas $V_{ext}[\rho]$ defines the system that is being studied, so it is known once $\hat{\mathrm{V}}_{ext}(\mathbf{r})$ is defined.

2.3.2 Kohn-Sham Method

Although the HK theorems give rise to using the electron density as a means to study many body systems, reducing the complexity of the problem of $4N$ variables to only 3, it did not provide a means on how to implement this in a practical manner. Not until the workings of Kohn and Sham [29]. Taking a route similar to what was done in the HF approximations, they introduced the Kohn-Sham (KS) orbitals, ϕ_{KS}, which are functions that are equivalent to spin orbitals, χ_i, that are used to build Slater determinants but whose absolute square sum gives ρ, as well as to provide a way to approximate the universal functionals in the following manner.

$$\begin{aligned} \rho(\mathbf{r}) &= \sum_{i}^{N} |\phi_{i,KS}|^2 \\ \mathrm{T} \approx \mathrm{T_S}[\rho] &= \left\langle \hat{\mathrm{T}} \right\rangle_{\phi_{KS}} \\ \mathrm{V}_{e,e} \approx \mathrm{J}[\rho] &= \frac{1}{2} \int \frac{\rho(\mathbf{r}_1)\rho(\mathbf{r}_2)}{|\mathbf{r}_1 - \mathbf{r}_2|} \, \mathrm{d}\mathbf{r}_1 \, \mathrm{d}\mathbf{r}_2 \end{aligned} \tag{2.22}$$

Where $\mathrm{T_S}$ is the kinetic energy of non interacting electrons and J is the HF formulation of the classical electron-electron repulsion. Thereby, the energy functional now has the following structure.

$$\begin{aligned} \mathrm{E}[\rho] &= \min_{\psi \to \rho} (T + V_{ext} + V_{e,e}) = \mathrm{T_S}[\rho] + \mathrm{J}[\rho] + \mathrm{V_{ext}}[\rho] + \mathrm{E_{xc}}[\rho] \\ \mathrm{E_{xc}}[\rho] &= (\mathrm{T}[\rho] - \mathrm{T_S}[\rho]) + (\mathrm{V}_{e,e}[\rho] - \mathrm{J}[\rho]) \end{aligned} \tag{2.23}$$

In which the exchange-correlation energy functional, $\mathrm{E_{xc}}$, has been introduced and contains the missing exact contributions of the kinetic energy of interacting electrons, as well as the exchange and correlation contributions of the interaction between electrons. So if we were to know the explicit form of $\mathrm{E_{xc}}$ or at least have a very good approximation of it, we would be able to calculate near to exact results of any many body system within the confines of the BO approximation. Unfortunately, we simply have not been able to achieve something similar to a universal $\mathrm{E_{xc}}$, instead there exist many functionals that are proven, in comparison with experimental data or exact so-

lutions, to obtain good results for specific subsets of molecular systems. Other ways have been to theoretically obtain them by physical approximations.

Finally, writing the energy functional 2.23 with the non-interacting orbitals and using the variational principle, constrained with the conservation of the total number of electrons, one obtains the KS equations that resemble the HF ones but with a local exchange-correlation potential, $\hat{\mathrm{V}}_{\mathrm{xc}}(\mathbf{r})$, replacing the non-local exchange potential.

$$\begin{aligned} &-\frac{1}{2}\nabla^2\phi_j(\mathbf{r}) + \hat{\mathrm{V}}_{\mathrm{ext}}\phi_j(\mathbf{r}) + \int \frac{\rho(\mathbf{r}')\phi_j(\mathbf{r})}{|\mathbf{r}-\mathbf{r}'|}\,\mathrm{d}\mathbf{r}' + \hat{\mathrm{V}}_{\mathrm{xc}}(\mathbf{r})\phi(\mathbf{r})_j = \epsilon_j\phi_j(\mathbf{r}) \\ &\hat{\mathrm{V}}_{\mathrm{xc}}(\mathbf{r}) = \frac{\delta \mathrm{E}_{\mathrm{xc}}[\rho]}{\delta\rho} \end{aligned} \tag{2.24}$$

As a reminder, the local exchange-correlation potential contains contributions from both the real kinetic energy of interacting electrons and that of exchange and correlation between electrons. It is exact if and only if $\mathrm{E}_{\mathrm{xc}}[\rho]$ is exact, but as stated beforehand, it is currently unknown. Additionally, although the orbitals are made from a Slater determinant, having exact knowledge of the exchange-correlation energy functional would compensate and make irrelevant the shortcomings of the mono-configurational approach[2] made during the construction of the KS orbitals. Thus, good approximations of $\mathrm{E}_{\mathrm{xc}}[\rho]$ are crucial for successful results.

2.3.3 Exchange–Correlation Functionals

Since the publication of the KS theorems, there have been many suggestions and approximations made for the exchange-correlation energy functional, all of which can more or less be classified into four groups or approaches; local density approximation (LDA), generalized gradient approximation (GGA), meta-GGA, and hyper-GGA or hybrid functionals. LDA was the first approximation to E_{xc}, and still used to this day. It is based on the exact kinetic and exchange energy of a non-interacting homogeneous electron gas, which was first studied by Thomas and Fermi [75, 12] and later expanded upon by Dirac [8] to include a local exchange energy contribution. Unexpectedly,

[2]This is true if and only if, the first excited states are sufficiently high in energy as to be unaccessible and therefore have a small contribution to the overall electronic structure

this approach reliably calculates molecular geometries, and vibrational frequencies for many systems, mostly in part to (i) a fortunate canceling of errors between the exchange and correlation energies and (ii) a reasonable description of the spherically averaged exchange correlation hole. The exchange correlation hole may be thought as the space, $\mathbf{r}_1$, in which an electron burrows itself reducing the probability of any other electron occupying any space around $\mathbf{r}_1$.

An improvement upon LDA functionals, GGA functionals are approximations based on expanding $\mathrm{E_{xc}}[\rho]$ in a Taylor series, taking LDA as the zeroth term and usually truncating the series on its first term. The exchange correlation energy now becomes a functional dependent on the electron density and its gradient, $\mathrm{E_{xc}}[\rho, \boldsymbol{\nabla}\rho]$. This increment of complexity gives way of introducing a degree of experimental parameters to some of its functionals (HTCH[21], BLYP[32]) although it is not totally necessary (PBE[56]). The latter sort of functionals are commonly known as pure functionals. Still the shortcomings of these last two approaches greatly affect their utility, both LDA and GGA functionals overestimate the magnitude of the exchange energy due to their locality, thus providing a path for improvement for future approximations.

Along the same lines of the GGA, meta-GGA functionals include dependency on both, electron density and its gradient, but betters the former approximation by including contributions from variations of the non-interacting electron kinetic energy $\tau(\mathbf{r})$,

$$\tau(\mathbf{r}) = \frac{1}{2}\sum_{i}^{occ} \left|\boldsymbol{\nabla}\phi_{i,KS}(\mathbf{r})\right|^2 . \tag{2.25}$$

Thereby τ is assessed by summing individually the non-interacting kinetic energy of the occupied Kohn-Sham orbitals. Whereby $|E_x[\rho, \boldsymbol{\nabla}\rho, \tau]|$ is lowered in comparison with the previously stated methods, LDA and GGA.

On the other hand, hybrid functionals are characterized to mix the exact exchange contribution from the HF approximation with other types of functionals, regardless if they are GGA functionals or LDA functionals, thereby decreasing the $|\mathrm{E_{xc}}|$. These functionals are also known to include some experimental parameters obtained by fit-

ting observed physical chemical values, e.g. electron affinities, ionization potentials, atomization energies, and total atomic energies for small molecules. Hybrid functionals usually give excellent results for many types of systems, one of the most important of such functionals is B3LYP [26, 70] for it has turned out to be the work horse for these type of functionals, useful for a myriad of systems. Although hybrid functionals are usually the better choice for many types of molecular systems, they demand much more computational processing compared wth the other functionals due to the introduction of the exact exchange contribution.

2.4 Configuration Interaction

The HF method determines the lowest energy configuration of an atomic system, with the given spin orbitals, such that it usually gives about 99% of the ground state energy; still this accuracy is not enough to be able to discern important physical-chemical properties such as bond and dissociations energies which usually have magnitudes that are well less than 1% of the total energy of a molecule or chemical system. As previously mentioned, one must thus adhere to finer methods that fix the correlation inadequacies that are at the foundation of the HF method. A solution would be to provide a better approximated wave function, one that includes different configurations apart from the mono-configuration used in HF calculations. The only reasonable additional configurations to add to a molecule's wave function are its excited states, examples of them from a singlet system can be observed in Figure 2-1. Normally, these excited states are of any sort, singly, doubly, triply, quadruply, etc., and their determinants are referred to as Singles (S), Doubles (D), Triples (T), Quadruples (Q), and so forth. Much like the influence a basis set has upon the quality of the molecular orbitals, the amount of excited states affects the quality of the approximated many body wave function. Theoretically, if the trial wave function, ϕ, is given by the following linear combination of SD determinants,

$$\phi = \sum_{i=0} a_i \Phi_i = a_0 \Phi_{HF} + \sum_{\mathrm{S}} a_{\mathrm{S}} \Phi_{\mathrm{S}} + \sum_{\mathrm{D}} a_{\mathrm{D}} \Phi_{\mathrm{D}} + \ldots, \tag{2.26}$$

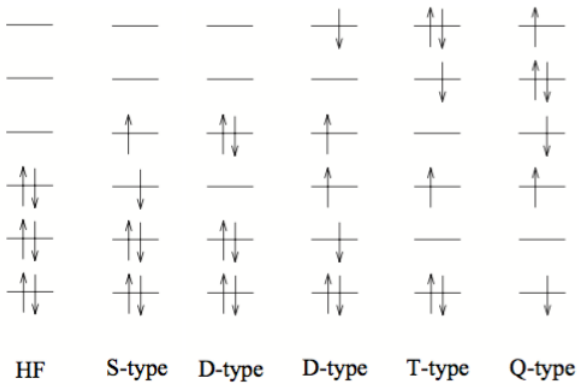

Figure 2-1: The excited configurations for a singlet molecule generated from the HF ground state configuration.

then, it is said to be the real ground state wave function when the orbital base is also complete, from which we would be able to obtain the exact energy given the BO approximations. It should also be noted that what is being summed are all the possible S-type, D-type, T-type, etc., excited configurations weighted by their respective coefficient a_i. Equation 2.26 is the explicit wave function of the Configuration Interaction (CI) method. Where it is usually admitted that if $|a_0|^2 \geq 0.70$, it is sufficient to use first principles calculations using mono-configurational methods, like DFT or HF. The absolute square of the CI coefficients represent how much of the respective configuration contributes to a molecule's ground state character.

As it can be inferred, this method is intractable for systems of more than a few atoms, thus, new approximations are needed for its usage in larger molecules now that the variational principle is needed to determine thousands of weighting coefficients. As an example of the method's intractability, if we were to set up a scenario in which we distribute k alpha (k_α) and k beta (k_β) electrons in $2k$ orbitals to see how the number of Slater determinants (N_{Det}) escalate by increasing the number of orbitals by two in two we obtain those values in table 2.1, where we have assumed $k_\alpha = k_\beta = k$. Thus, $N_{Det} = \binom{2k}{k}\binom{2k}{k}$. So just by considering a case for when we place the number of electrons of a small molecule like molecular oxygen (O_2), 16 electrons, that permeates our entire atmosphere, within the same number of orbitals. We observe that the number of possible determinants is in the 2 thousand millions mark,

incredibly large for such a small but essential molecule on our planet. Consequently, it is out of the question to study conjugated systems without further simplifying this method. Typical ways of reducing the method's complexity rely on truncating the linear combinations to a certain batch of excited states, or by selecting configurations that may be thought to sufficiently describe the molecular system or a property of interest.

Table 2.1: Number of Slater determinants N_{Det} per the ways $2k$ electrons may be distributed in $2k$ orbitals.

2k	N_{Det}
2	4
4	36
6	400
8	4,900
10	63,504
12	853,776
14	11,778,624
16	165,636,900
18	2,363,904,400
20	34,134,779,536

2.5 Multi-Configurational Self Consistent Field

Unlike the way in which the spin orbitals are treated in CI calculations, they are also optimized by the variation principle in multi-configurational self consistent field (MCSCF) methods, 2.27. This makes this approximation much more restrictive with respect to the size of the chemical compounds it can handle, also, unlike the CI approach, complicating the minimization of its energy functional. The concerning equations now being highly non-linear, thus necessitating the inclusion of an spin orbital rotation operator, $e^{-\hat{\Omega}}$ that conserves the symmetry constraints during the non linear minimization procedure, such as well defined wave functions with honest

spin quantum numbers.

$$\begin{aligned} \phi &= e^{-\hat{\Omega}} \sum_{i=0} a_i \Phi_i \\ \mathrm{E}[\phi] &= \min_{\Omega, a} \left(\frac{\int \phi^{\dagger} \hat{\mathrm{H}} \phi \, \mathrm{d}\tau}{\int \phi^{\dagger} \phi \, \mathrm{d}\tau} \right) \end{aligned} \tag{2.27}$$

Although limited, this method is also useful when mono-configurational methods come up short, as well as treating open shell problems that do not include spin contamination corrections. Therefore, this method improves upon the HF and DFT methods by introducing a greater contribution of static correlation, whereupon hand picked configurations that are believed to be the important ones are included, with which the determinants are constructed. Overall, these methods are used for obtaining qualitatively correct wave functions, with most of the static correlation included, subsequently providing the correct spin-orbitals for further analysis of dynamical correlation by additional methods.

2.5.1 Complete Active Space Self Consistent Field

As an MCSCF method and an approximation to the full CI method, complete active space self consistent field (CASSCF) relies on a selection of available electrons (n) and orbitals (m) with which all CI configurations are created, thus deemed as the active space, whereas the inactive molecular orbitals are doubly or non occupied (virtual orbitals) and left alone during the optimization of the CI coefficients and spin orbitals. This method still needs HF as an initial guess to start the calculation or it can also use outputs from other CASSCF calculations. That being said, the final results given are the optimized CI coefficients and the ground state energy of the molecule under study. A common notation is CASSCF(n,m), which indicates that n electrons are distributed in all possible ways in m orbitals. A schematic example of a CASSCF(8,8) active space can be found in Figure 2-2. In the case of taking all electrons and orbitals of a molecule to be the active space, would only translate the CASSCF method to the full CI method.

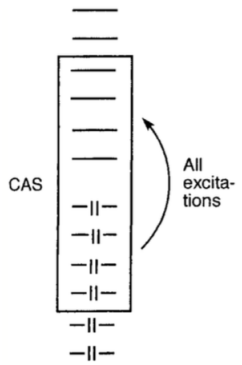

Figure 2-2: Diagram representing a CASSCF-(8,8) calculation with its respective active electrons and orbitals.

2.6 Restricted & Unrestricted Models

Up until now we have not talked about the type of molecular systems we have addressed in this but rather have kept it quite general with respect to the number of electrons and nuclei in preceding sections. Now the task in hand is to explore how the spin orbitals may be distributed in molecules and how they are dealt with, especially with what happens when we do not deal with an even number of electrons. Which cannot be represented by an square (NxN) matrix.

It is common to think that the way electrons are distributed in their molecular orbitals is done so by filling them up such that two electrons occupy the same spatial function, their spin configuration being what sets them apart. In other words, many times it is supposed that if we have N molecular orbitals for a system of N electrons, only the bottom half of the orbitals would become occupied, being representable by an NxN matrix. This is what is known as a closed shell singlet or restricted model, and is common for most molecular systems. There are others in which one or more electrons can be unpaired in a molecule's ground state, thus providing the need to implement another approach now that there is a disparity between $\alpha(s)$ and $\beta(s)$ electrons. The unrestricted and open shell models provide a means of correcting this issue by separating the electronic problem in two and treating individually the electrons of different spin. Hence, they do not share the same external potential, rather $\mathrm{V}_{ext}^{\alpha}$, and V_{ext}^{β}, neither do they share the same spatial characteristics.

Although it may seem as though we are now dealing with a multi determinant method, the one determinant has only been divided into two contributions, much like the way most matrices can be made symmetrical or anti-symmetrical. The unrestricted models also help with the inclusion of certain correlation by becoming contaminated with other configurations, but simultaneously deviate of the $\left\langle \hat{\mathrm{S}}^2 \right\rangle = \mathrm{S}(\mathrm{S}+1)$ values as it also encompasses configurations of higher spin multiplicity. The spin contamination can be addressed using the following equation which considers non-interacting electrons, much like in the case of DFT or HF spin orbitals, but in this case is intended for the DFT KS orbitals [7],

$$\left\langle \hat{S}^2 \right\rangle_{NI} = S(S+1) + N_\beta - \sum_i^{N_\alpha} \sum_j^{N_\beta} | \int \phi_i^{\alpha,*}(\mathbf{r}) \phi_j^{\beta}(\mathbf{r}) \, \mathrm{d}\mathbf{r} \, |^2. \tag{2.28}$$

Where NI stands for a non interacting system, and $S = (N_\alpha - N_\beta)/2$ is the net spin of a molecular structure with N_i either being the number of spin up (α) and spin down (β) electrons. Here ϕ_i^α and ϕ_j^β are the orbitals coming from the spin-unrestricted case with spin up and down, respectively. Then, if the ϕ_i^α and ϕ_j^β orbitals are identical in the singlet ($S = 0$) ground state, there will be no spin contamination, and the unrestricted wave function is identical to the restricted one. This equation also offers a way to quantify the contribution of higher spin states to the $\left\langle \hat{\mathrm{S}}^2 \right\rangle$, specifically for DFT calculations, which will become of use during our discussion of the obtained results of silicene nanoribbons.

Chapter 3

Silicene Nanoribbons

In this thesis we report our findings of the electronic properties of silicene nanoribbons with hydrogen passivated edges denoted by H-SiNRs(n_z, n_a), with n_z and n_a representing the zigzag and armchair directions (Fig. 3-1), respectively. For example, H-SiNR(1,1) and H-SiNR(2,1) stand in for silicon structures analogous to benzene and naphthalene, respectively. In order to verify the influence of the two parameters, n_z and n_a, in the the electronic properties of these systems, we increased their lengths by one additional ring at a time. Furthermore, the need to terminate the dangling edge bonds with hydrogen was brought on by the lack of convergence of these systems and thus an indication of their chemical irrelevance; certainly due to the destabilization provided by the excess of unpaired electrons in the system and by the increase of the amount of permitted multiplicities in the system.

3.1 Computational Details

As mentioned in chapter 1, the need to consider the effect of electronic correlation of the H-SiNRs was apparent, therefore, by using multi-configurational first principles calculations, where CASSCF was employed, we were able to take static correlation into account. Additionally, we chose the Beck 3-Parameter (exchange), Lee, Yang and

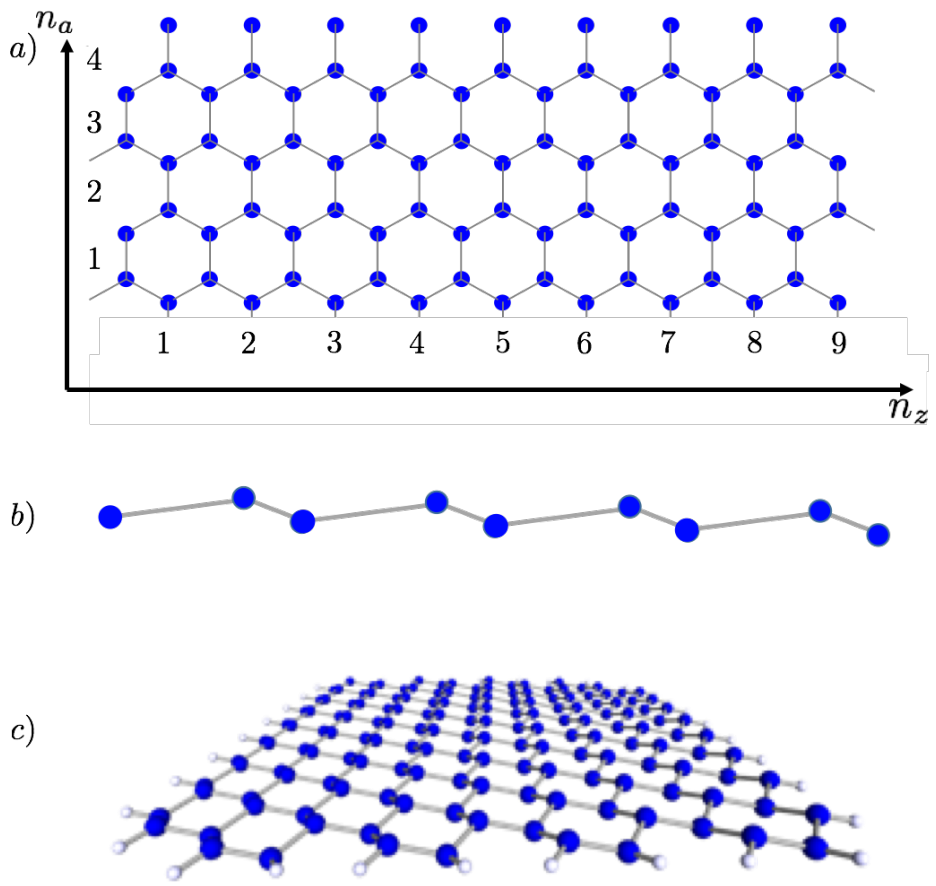

Figure 3-1: Top (a) and side (b) views of the silicene structure H-SiNR(9,4), and (c) the optimized geometry of an H-SiNR(8,8) structure, where the edges are passivated with hydrogen in the DFT(B3LYP) level of calculation.

Parr (B3LYP) functional[1] with the correlation consistent polarized valence double zeta (cc-pVDZ) basis pairing (B3LYP/cc-pvDZ) along with D3 dispersion correction [18] which was applied to study H-SiNRs using TURBOMOLE V7.0 [1]. The basis selection was due to its ability to account for some correlation energy of the valence electrons in molecules, as well as not being too computationally demanding. Thus, we performed geometrical optimizations of H-SiNRs and afterwards we analyzed the triplet instability of the Kohn-Sham (KS) wave function. In this case, an instability is the lowering of the molecule's total energy by variation of the occupied molecular orbitals that have subsequently been optimized to satisfy certain constraints, e.g. spatially doubly degenerate spin orbitals as in closed shell calculations. The variation of the occupied spin orbitals is done by replacing an occupied one with a virtual one. This analysis was also done with TURBOMOLE V7.0 whose method divides the energy variation with respect to the occupied orbitals into the following three terms:

$$\delta E = \delta E_N + \delta E_1 + \delta E_2 \,.$$

Where δE_N denotes the variation of the electron kinetic and nuclear attraction energies, δE_1 and δE_2 collect the linear and quadratic terms of the variation of the electron density, respectively, which emerge from the Coulomb and exchange-correlation contributions to E. Upon a unitary transformation of the previous equation, δE is then split into two matrices, A and B, that may have positive or negative eigenvalues for the optimized spin orbitals under analysis. Consequently, if the matrices are only comprised of positive eigenvalues, these orbitals provide the lowest expectation value of the ground state Hamiltonian within the constraints considered. On the contrary, a negative eigenvalue in either matrix, A or B, would indicate an instability related to the symmetry constraints imposed from the onset of the calculation; a negative eigenvalue in matrix A is known as the singlet instability and states that a decrease in energy is possible by using complex spin orbitals but still maintaining doubly occupied orbitals, $\phi^\alpha = \phi^\beta$. Whereas, a negative eigenvalue in matrix B is known as

[1] we chose to use this functional due to it outperforming the PBE and M026x functionals which can be consulted in appendix A.

the triplet instability and indicates that there exists a lower energy configuration of the molecule by breaking the orbital degeneracy, $\phi^{\alpha} \neq \phi^{\beta}$, and/or deeming its ground state a triplet spin state. Thus, upon encountering the latter type of instability, we removed the closed shell approach and employed the open-shell unrestricted broken symmetry (UB) method to re-optimize the geometry of the singlet state in order to find the correct total spin for the ground state. In addition, we used the CASSCF method (as implemented in Gaussian09 [15]) with an active space of ten orbitals and ten electrons to determine the multi-configurational character, and to determine whether or not mono-referential wave functions are efficient to describe the H-SiNRs thus obtained. MCSCF methods are computationally very demanding as stated in chapter 2, so we maintained the same active space for all molecules, invariant of their size. Lastly, from the optimized geometries, the non-resonance Raman spectra were calculated for the singlet and triplet states of H-SiNRs, that can be used as a means to detect these structures experimentally.

3.2 Results & Analysis[2]

We again mention some important features regarding spin contamination and electron correlation while using the unrestricted formalism, to better understand the multi-configurational character of the H-SiNRs(n_z, n_a) structure. A spin-unrestricted wave function for a given spin state can be written as a linear combination of the pure-spin wave functions plus contributions from higher spin states, resulting in an expectation value for the $\hat{S}^2$ operator that exceeds the exact $S(S+1)$ value, because the contaminants tend to have large values of S. In particular, spin contamination for any single-determinant spin-unrestricted wave function can be evaluated using equation 2.28.

In Table 3.1, the computed relative energies for singlet and triplet state, and their respective spin squared expectation values, $\langle \hat{S} \rangle_{NI}$, are shown. All values are reported in kcal per mol for the calculated states, and the relative energies from Table

[2]This has already been reported in [53]

Table 3.1: Relative energies in kcal/mol of the open shell triplet (S_1-UB3LYP) and the open shell singlet (S_0-UB3LYP) states with respect to the restricted shell singlet S_0-RB3LYP. The corresponding $\langle \hat{S}^2 \rangle_{NI}$ expectation values are also shown for various (n_z, n_a) silicene ribbons. The subscript NI here denotes a non-interacting system.

H-SiNR(n_z, n_a)	N	S_1-UB3LYP	$\left\langle \hat{S}^2 \right\rangle_{NI}$	S_0-UB3LYP	$\left\langle \hat{S}^2 \right\rangle_{NI}$
(1,1)	1	0	0	0	0
(2,1)	2	0	0	0	0
(3,1)	3	0	0	0	0
(4,1)	4	8.696	2.06	-0.182	0.47
(5,1)	5	4.579	2.07	-1.418	0.92
(6,1)	6	1.717	2.08	-3.103	1.23
(7,1)	7	-0.306	2.09	-4.910	1.50
(2,2)	4	0	0	0	0
(3,2)	6	0	0	0	0
(4,2)	8	4.899	2.12	-0.974	0.81
(5,2)	10	0.806	2.13	-3.067	1.20
(6,2)	12	-2.086	2.16	-5.451	1.54
(7,2)	14	-4.181	2.22	-7.854	1.85
(3,3)	9	8.517	2.10	0.000	0.30
(4,3)	12	1.598	2.12	-2.076	1.08
(5,3)	15	-3.015	2.15	-5.334	1.40
(6,3)	18	-5.914	2.17	-8.381	1.69
(7,3)	21	-7.636	2.19	-11.196	2.11
(4,4)	16	-0.368	2.16	-2.993	1.22
(4,5)	20	-2.164	2.19	-3.976	1.32
(4,6)	24	-13.423	2.22	-14.723	1.38
(4,7)	28	-4.799	2.25	-5.718	1.41
(4,8)	32	-5.793	2.28	-6.462	1.41
(4,9)	36	-11.663	2.31	-12.154	1.43
(5,4)	20	-5.253	2.19	-6.877	1.48
(6,4)	24	-8.093	2.22	-10.197	1.85
(7,4)	28	-9.564	2.27	-13.185	2.31
(7,6)	42	-12.480	3.31	-16.003	2.61

3.1 are given with respect to their corresponding closed shell singlet state energy (S_0-RB3LYP). The systems in this table that only register zeros did not show a triplet ($S = 1$) state instability in their closed shell state wave function and therefore calculations using the UB3LYP method were not pursued. As seen from Table 3.1, the energies for the open-shell species, (S_0-UB3LYP) and (S_1-UB3LYP), always are lower than their corresponding RB3LYP energies for $N \geq 15$. Where N is the total number of rings that comprise a system, ($N = n_z \cdot n_a$). This energy decrease arises from from different causes, for instance, the use of different orbitals for each electron allows the α and β electrons to be more spatially separated on average than in a RB3LYP wave function and introduces some correlation between orbitals of different spin whence using unrestricted methods[27]. But in some cases, the mixing of higher spin states usually causes the energy to increase and may destablize the molecule. So, when electron correlation is included, the deviation of $\langle \hat{S}^2 \rangle$ from $S(S+1)$ is simply due to the mixing of higher spin states. Therefore, since UB3LYP introduces electron correlation to a certain extent, the values of $\langle \hat{S}^2 \rangle$ presented in Table 3.1 suggest the presence of higher spin states. The stability of the H-SiNRs is examined by comparing the energies of the singlet and triplet states. From the results thus obtained, we can observe that the ground state is given by the singlet state for $n_z > n_a$ because of how the energy difference between the two multiplets. Along the n_a direction, the energy difference between the singlet and triplet states becomes closer to zero for $n_a > n_z$. The closeness in energy between S_1-UB3LYP and S_0-UB3LYP states could indicate a transition for the ground state from a S_0 to a S_1 multiplet as n_a increases. However, the energy differences for $n_a > 6$ between the single and triple states at the DFT level of calculation are not decisive because the results are within the accuracy limits of DFT.

Now we discuss the magnitude of the spin contamination $\langle \hat{S}^2 \rangle$ for the singlet and triplet states. Figures 3-2(a) and 3-2(b) illustrate the deviation of the average $\langle \hat{S}^2 \rangle$ values from their eigenvalues $S(S+1)$ for $S = 0$ and $S = 1$ in the zigzag and armchair directions, respectively. Figures 3-2(a) and 3-2(b) show that the $\langle \hat{S}^2 \rangle$ values for the singlet state is the most seriously contaminated in comparison with the triplet state,

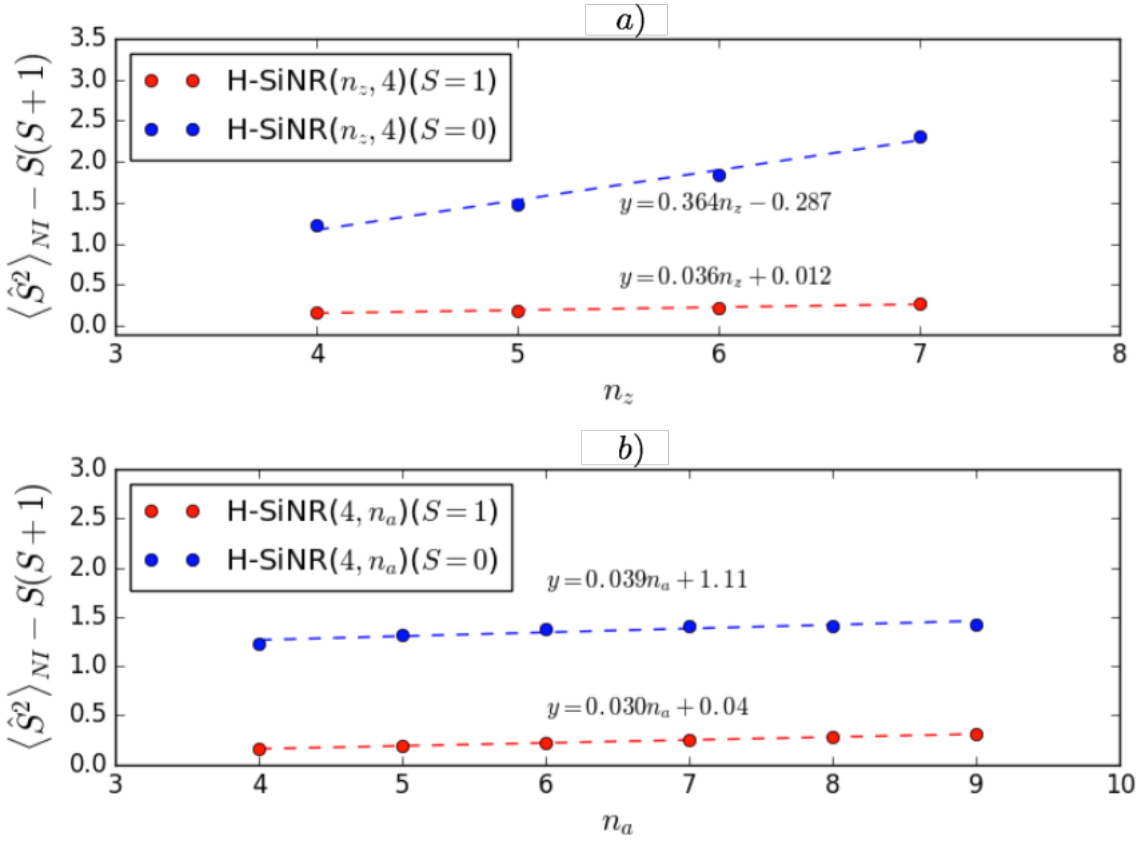

Figure 3-2: Deviation of $\langle \hat{S}^2 \rangle_{NI}$ values from $S(S+1)$ as a function of the length of the ribbon in the (a) zigzag n_z and (b) armchair n_a direction, respectively. The plotted results are taken from Table 3.1.

indicating that the wave functions for the singlet state were severely contaminated with higher spin states. Furthermore, we observe that the spin contamination is greater in the zigzag direction than in the armchair direction for the singlet state, with a ratio of $9.3 \times n_z/n_a$ found from the two linear regressions. For the triplet state, the spin contamination increases almost at the same rate for both the zigzag and armchair directions with a ratio of $1.2 \times n_z/n_a$, indicating that the spin contamination is smaller in the triplet state than in the singlet state.

It has been previously reported that similar sets of nanoribbons but of graphene have shown antiferromagnetic ordering of the electrons spin on the zig-zag edges and with an anti-ferromagnetic ordering between the two zig-zag edges[16, 48]. Consequently, we calculated the spin density distribution of the singlet and triplet multiplets of H-SiNR(4,7), H-SiNR(4,8) and H-SiNR(4,8), having in mind to observe whether

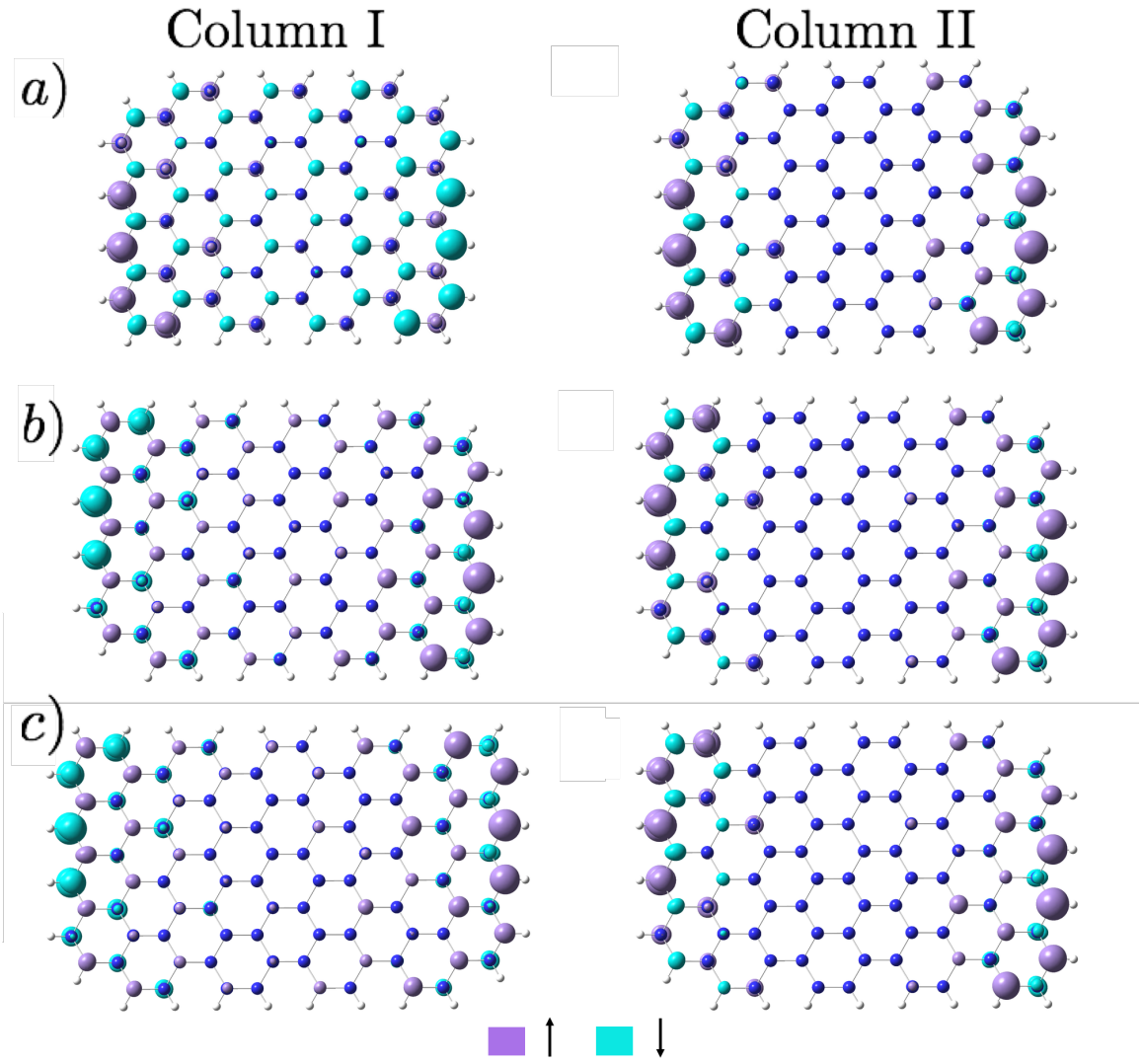

Figure 3-3: Spin densities of the (column I) singlet and (column II) triplet of a) H-SiNR(4,7), b) H-SiNR(4,8) and c) H-SiNR(4,9); the colored boxes indicate the (up and down) spin directions of the respective spin densities.

these ordered states are also present. According to figure 3-3, the previously stated orderings do occur and interestingly, the triplet states present ferromagnetic ordering between the edges, whereas, the singlet multiplets have the anti-ferromagnetic coupling between both edges. The fact that ferromagnetic coupling is accesible without an external perturbation is surprising, taking into account that a parallel electric field with respect to n_a is necessary for the appearance of this ordering in graphene [68], while we get it for free with these silicene structures. Upon further analysis of the three singlet spin densities, it can be seen that there are more localized spin states toward the middle of the molecules in comparison with the the other multiplicity. This interesting feature must confer the singlet systems with greater exchange energy than the triplet systems, thus stabilizing them. But it can readily be seen that as we increase the distance between the edges, the intermediate localized spin states start to disappear, therefore, indicating an interaction between the localized spin edge states. In fact, this phenomena has already been reported and explained for graphene nanoribbons [16], where these localized spin states decay into the inner atoms by traveling exclusively through the same type of sublattice atom it originated from. Moreover, due to the way these states decay, if the system is composed by an anti-ferromagnetic coupling between both zig-zag edges, constructive interference occurs on the atomic sites with respect to the type of spin density and it is for this reason, in the case for the singlet systems, there are more localized spin states in the middle region of our silicene systems. On the other hand, the opposite (destructive interference) occurs when a ferromagnetic ordering is present between the localized edges. But because these states have finite decay lengths, we can prevent interference from happening with a large enough separation between the edges, which can be inferred from the spin densities in figure 3-3 and which would further influence the ground state of these systems. A study concerning graphene nanoribbons, using the tight binding approximation (a method that neglects electron-electron interactions), indicates that by eliminating the aforementioned interactions by larger separations, the ferromagnetic and anti-ferromagnetic molecules would become degenerate with respect to their ground state energies [33], much like the transition we report here. Experimentally,

it has been reported [40] that graphene nanoribbons under ambient conditions transition from anti-ferromagnetic to a ferromagnetic zig-zag edge coupling, along with the closure of the nanoribbon's band gap, for zig-zag edge separations of more than 7 nm. The latter may be due to the ambient temperature under which the measurements were made and as we will see, are not reflected in our HOMO-LUMO (H-L) gap values but this too may be a product of our 0 K calculations. Additionally, these observed localized states are formed by the overlapping of the valence and conduction band on the zig-zag edge states, as explained for graphene nanoribbons', they are also known as metallic edge states[16], and which gives rise to the anti-ferromagnetic ordering but of unequal magnitude, originating ferrimagnetic properties. Ferrimagnetic states must not be confused with ferromagnetic states, both present an inherent non zero magnetic field but much like the case in antiferromagnetic states, neighbouring sites present antiparallel magnetic moments with one moment greater in magnitud than the other (Fig.3-3). The relevancy of these type of materials is that they could be used in magnetic memory devices because of the presence of states with vanishing angular and magnetic moments below its Curie temperature [69]. Furthermore, the excess of zig-zag edge states in these systems affects their overall stability, as $|\text{E(H-SiNR}(n,m))|>|\text{E(H-SiNR}(m,n))|$ for $m > n$. The latter is understood to be a consequence of prohibiting aromatic states around the zig-zag edges, whereas, the armchair edges do not originate such limitations.

Due to the detection of higher spin states with the single determinant spin unrestricted wave functions (see Table 3.1), we use multi-referential first principles calculations, in this case, using the CASSCF(10,10) method with a 6-31G(d) basis set. We were thus able to obtain energies for the different optimized multiplets, along with their respective configuration-interaction (CI) coefficients for different configurations and consequently, we can obtain the most representative configurations, see Table 3.2. When the number of total rings is greater than 16 (N>16), it appears that subsequent H-SiNRs are equally likely to have both triplet and singlet ground states, and this is represented physically by a very small energy difference between them. However, when $n_a > n_z$, we observe that the triplet state is more stable than the

Table 3.2: Relative energies [kcal/mol] and greatest squared CI expansion coefficients of dominant configurations obtained by the CASSCF(10,10) method for both the $S = 0$ and $S = 1$ states. The relative energies were calculated with respect to the singlet state reference.

H-SiNR(n_z, n_a)	N	CI		Relative
		S = 0	S = 1	Energy(S=1)
(1,1)	1	0.78	0.56	33.019
(2,1)	2	0.65	0.49	24.304
(3,1)	3	0.67	0.65	16.151
(4,1)	4	0.60	0.63	9.474
(5,1)	5	0.47	0.61	4.430
(6,1)	6	0.48	0.65	3.438
(7,1)	7	0.54	0.65	5.447
(2,2)	4	0.74	0.58	24.742
(3,2)	6	0.71	0.68	20.088
(4,2)	8	0.64	0.69	5.362
(5,2)	10	0.66	0.72	9.956
(6,2)	12	0.40	0.70	0.547
(7,2)	14	0.42	0.73	0.455
(3,3)	9	0.71	0.68	20.066
(4,3)	12	0.67	0.70	2.261
(5,3)	15	0.36	0.67	0.277
(6,3)	18	0.38	0.72	0.235
(7,3)	21	0.33	0.65	0.138
(4,4)	16	0.71	0.70	6.567
(4,5)	20	0.39	0.74	0.099
(4,6)	24	0.36	0.69	0.134
(4,7)	28	0.35	0.69	-0.004
(4,8)	32	0.35	0.69	-0.008
(4,9)	36	0.38	0.75	-0.050
(5,4)	20	0.40	0.77	0.102
(6,4)	24	0.36	0.71	0.014
(7,4)	28	0.34	0.67	0.047
(7,6)	42	0.37	0.75	0.022

singlet state as n_a increases, indicating that a transition from a singlet to a triplet ground state is likely. For $n_z > n_a$, the most stable state is the singlet state which can also be observed by reviewing the relative energies contained in 3.1. It is well known that as any chemical system's multiplicity increases, its multi-configurational character becomes less relevant up to the point of being successfully described by its dominant configuration. Thus, for $N > 12$ the square of the CI expansion coefficient for the $S = 1$ state exceeds 0.65, indicating the dominance of almost a single reference character for that multiplicity. In contrast, for the $S = 0$ state, the CI expansion coefficient squared does not even exceed 0.5, suggesting a multi-referential character. The dominant configurations then are 2222200000 and 2222$\alpha\alpha$0000 for the singlet and triplet states, respectively. The dominant configurations represent the electron distribution in the active orbitals and α represents positive 1/2 spin state.

Using Raman spectroscopy, we try to understand the multi-configurational character of H-SiNRs(n_z, n_a) along the zigzag and armchair directions and to provide a means for their experimental detection. Consequently, we proceded to calculate their non-resonant Raman spectrum, we carried out density functional calculations using UB3LYP with Dunning's correlation[18] consistent cc-pVDZ basis set. The interpretation of the silicene Raman spectrum is based on previously reported experimental data [81], along with the established analysis done for graphene, and using the calculated the phonon dispersion curve of silicene as presented in the Yan et al reference [79]. Before continuing it is important to state what is it that Raman spectra probes and its usefulness for the identification of materials.

Raman spectroscopy relies on the inelastic scattering of coherent light, such as from a laser of defined wavelength, irradiated upon a material that is polarizable – induction of an electric dipole or separation of electric density through interaction of light – and which couples with its vibrational degrees of freedom. If the material under study is not polarizable or if under the experimental ambient conditions the the material's dipole moment is already at an maximum before irradiance then no spectra would be obtained. Thus Raman spectroscopy informs us of how deformable the electron density of the atomic surface layers of a solid or of a thin film are with

respect to irradiance and is usually very effective for covalent bonding structures. Using the previous statements we produce a mathematical expression that quantifies the Raman effect of any material by expanding the polariizability by a Taylor's series.

$$\alpha = \alpha_0 + \sum_k \left(\frac{\partial \alpha}{\partial Q_k} \right)_0 Q_k + \cdots$$

Where α is the polarizability and Q_i is the i-th vibrational mode of a compound. Therefore, the Raman effect, in a very simplified explanation, is the projection of how an atomic system's polarizability varies with respect to its unperturbed geometrical configuration upon its available vibrational modes. What is more, there is an intimate relationship between the deformity of the electron clouds with the motion of the nuclei, wherein quantum mechanics, the nuclei vibrational modes are reduced to vibrational quanta known as phonons; there are principally two types of phonons, acoustic and optical. Acoustic phonons are those in which the nuclei move in the same direction of the propagation like sound waves, in other words, they move coherently or in phase. Whereas, optical phonons are only present when there are two or more atoms in a crystal array where adjacent nuclei move against each other (out of phase) just like oppositely charged ions in a homogenous electric field. Between the two types of phonons, optical phonons are of higher energy and can only be accessible beyond a certain energetic threshold. Both modes are given by dispersion relations which relates the phonon's energy with its wavevector (k). Additionally, there are also two subclassifications of phonons known as longitudinal and transversal modes, respectively, and describe the relationship of the atom's displacement with respect to propagation of the perturbation.

The dispersion relation obtained for free-standing silicene indicates phononic behavior similar to that of graphene, where the present modes reflect the stretching and bending of sp^2 bonds and other vibrational phenomena associated to modes that involve impurities and/or boundary bonds. Consequently, the following analysis concerning our systems are done in comparison to graphene, as well as using typical notation for graphene.

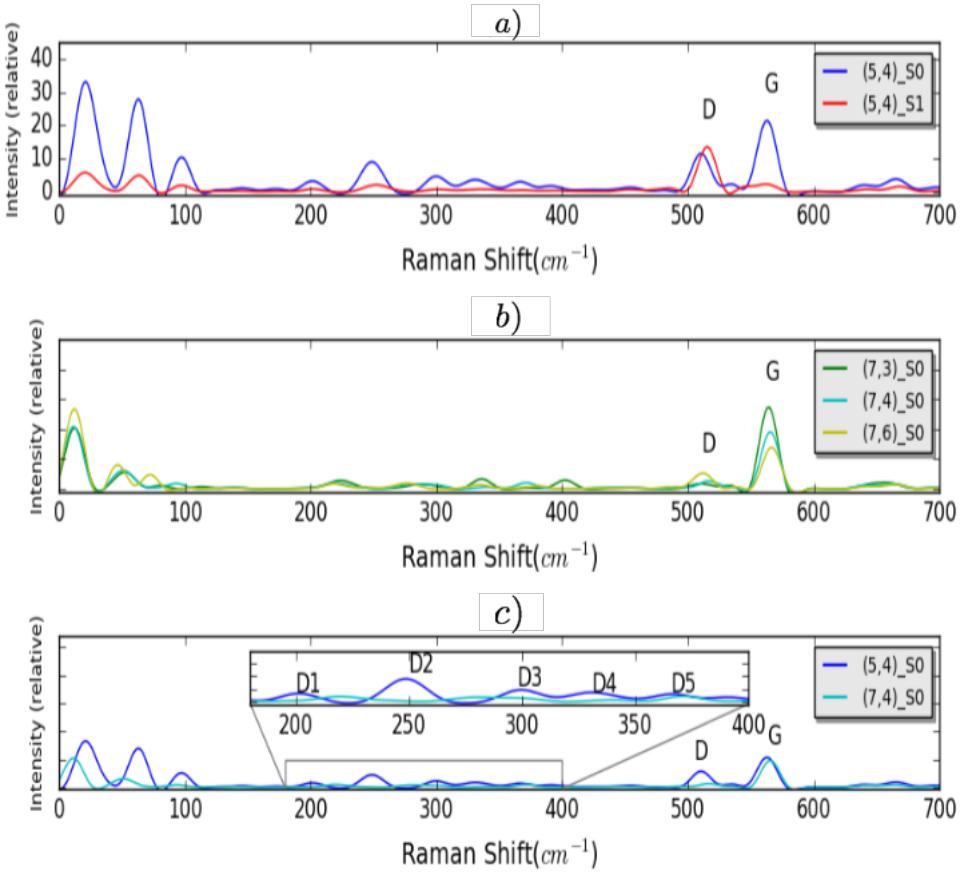

Figure 3-4: Raman spectra (Color line) of different H-SiNRs obtained by the calculated vibrational spectrum convoluted with a uniform Gaussian broadening having a 10 cm^{-1} width. (a) Raman spectra for the triplet and singlet states of H-SiNR(5,4). (b) Raman spectrum of H-SiNR(7,n_a) as a function of n_a. (c) Raman spectra of H-SiNR(n_z,4) as a function of n_z. The inset graph shows an expansion of Fig. 3-4(c) for the frequencies at around 200-400 cm^{-1}.

In Fig. 3-4(a), we show the Raman spectrum for the H-SiNR(5,4)-S_0 and H-SiNR(5,4)-S_1 states, respectively. The Raman spectrum for the S_0 state presents two high intensity peaks around 563 cm^{-1} and 512 cm^{-1}. The 563 cm^{-1} frequency is a doubly degenerate E_g (G peak) mode, which corresponds to the in-plane transverse optical (iTO) and the in-plane longitudinal optical (iLO) phonon branches at the Γ point (center of the Brillouin zone, $k = 0$), which have also been reported to be theoretically Raman active in silicene[79]. The G peak may also be seen as stretching relative to the motion of the horizontal sp^2 bonds, this peak is also present in bulk silicon but is nearly lower by 50 cm^{-1}. The other frequency 512 cm^{-1} represents the A_1 (D peak) mode which originates from the ribbons' edges and can be visualized as the breathing mode in which all atoms of a ring stretches radially outward with respect to the center of the ring. However, in graphene nanoribbons, only armchair edges are capable of elastically scattering charge carriers that give rise to the D peak [3]. The presence of this peak in graphene can also correspond to the presence of defects in its structure [59, 13]. Furthermore, we can notice a peak at around 665 cm^{-1} which is due to a vibration of the Si-H (1.5 Å) bonds at the edge of the ribbons. The intensity of this peak decreases with the width of the ribbon in the zigzag direction, which can then be used to determine the H-SiNRs width experimentally. Additionally, we observe other frequencies at around 200-400 cm^{-1} indicated in the inset graph of Fig. 3-4(c) which will be explained later on. The Raman spectrum for the triplet state (S_1) simply shows an intensive peak at around 516 cm^{-1} which corresponds to the symmetry-breaking D mode. In figure 3-4(b), we now explore the effect of increasing the number of fused rings in the n_a direction. As n_a increases the ratio of the relative intensity of the D and G peaks, $I(D)/I(G)$, increases, indicating that for $n_a > n_z$ the D peak will have a high intensity. In Fig. 3-4(c), we keep constant n_a and change n_z which shows that the intensity of the D peak decreases as n_z increases. However, the intensity of the G peak remains almost constant. The inset graph in Fig. 3-4(c) shows the $D_1 - D_5$ peaks which are attributed to electron inter- or intra-valley scattering at zigzag and armchair edges [59, 4] that involve two or more scattering stages. Comparing Fig. 3-4(b) and 3-4(c), it is likely that the intensities of

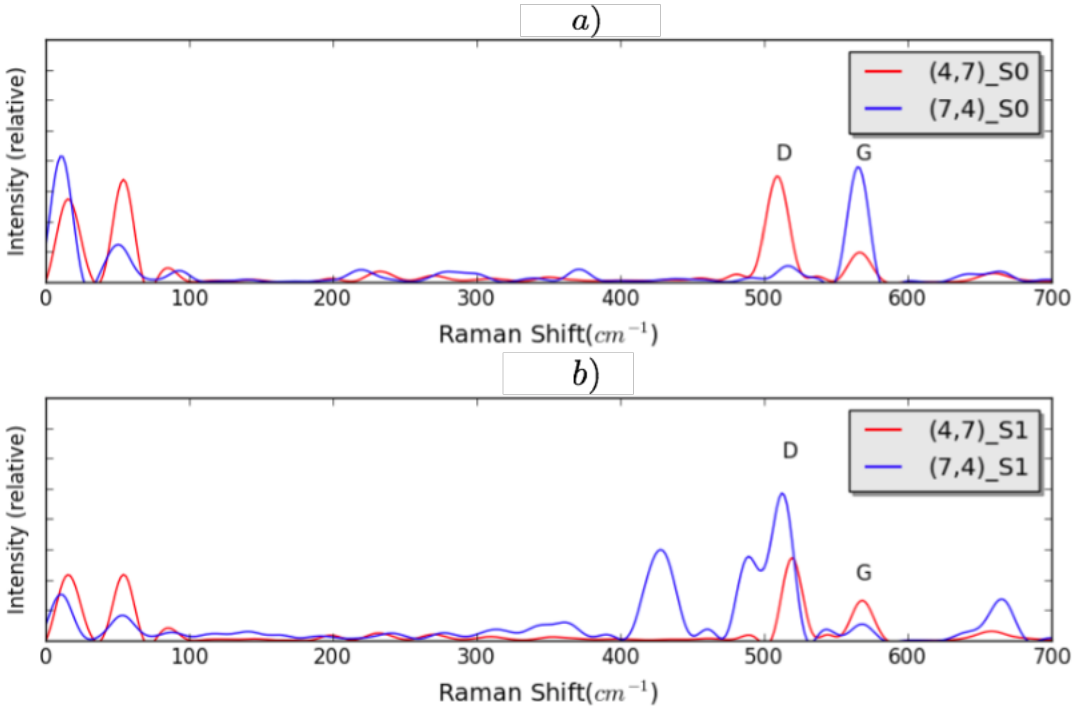

Figure 3-5: Raman spectra (Color line) of two H-SiNRs obtained by the calculated vibrational spectrum convoluted with a uniform Gaussian broadening having a 10 cm^{-1} width. (a) Raman spectra for the singlet states of H-SiNR(7,4) and H-SiNR(4,7). (b) Raman spectrum of of the previous systems but in their triplet states.

these peaks are associated with the armchair edges. Consequently, it is expected that more vibrational modes are induced for $n_a > n_z$. In the low frequency regions of all Raman spectra at around 20-100 cm^{-1}, we find other active peaks which correspond to the out-plane acoustic (ZA) phonons. This is because of the buckled structure of silicene which breaks the reflection symmetry with respect to the atomic plane, thus generating strong ZA phonons. The intensity of these peaks decrease with the width of the ribbon in the zigzag direction while they remain somewhat constant for a fixed n_z as shown in Figs.3-4(b) and 3-4(c). Thus according to the previous results shown in Tables 3.1 and 3.2, the triplet state can be observed for $n_a > n_z$ as shown in the Raman spectra for H-SiNR(4,7) in Fig. 3-5. Which ultimately agrees with our CASSCF calculations concerning these states previously mentioned. We also observe that the extra peak in the triplet state of the H-SiNR(7,4) can be conferred to excited states such as scattering between electrons and phonons, whereas these extra peaks

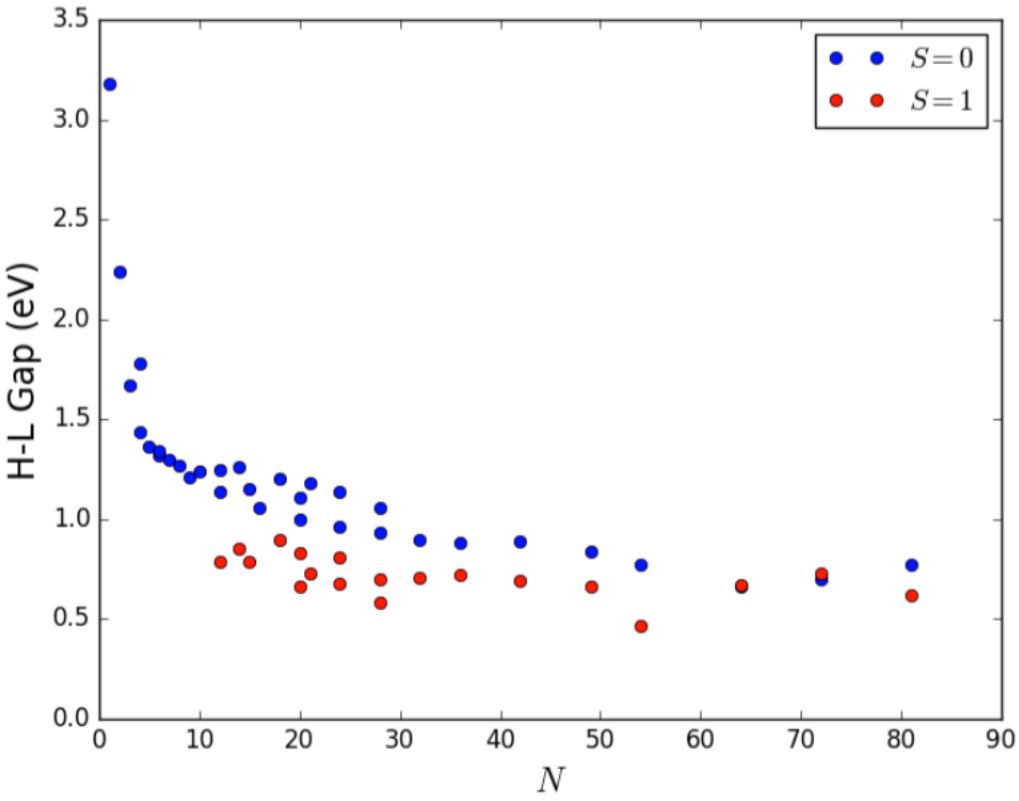

Figure 3-6: H-L gap (Color line) in eV for H-SiNRs as a function of N.

are not seen in the H-SiNR(4,7)'s triplet state, confirming our reason to believe that indeed its ground state is given by such multiplicity.

As previously mentioned, it is considerably difficult to synthesize silicene but Zhuang et al [81] have reported the detection of the G peak of silicene on a Ag substrate. They reported the G peak to be at 530 cm^{-1} and for their sample to have bond lengths of $2.32 - -2.38$, whereas, ours are within the interval $2.22 - -2.29$ which are in the range of other publications concerning free standing silicene [54, 80]. Therefore, Zhuang et al have then concluded that there must be some electronic coupling between silicene and its substrate to be able to explain the discrepancy between their reported values and those in previous theoretical studies.

Another relevant property for the usage of this material in novel electronic devises is its band gap, but due to the small sizes of our systems we can only talk about its H-L gap. The corresponding calculated H-L energy gap has been plotted as a function of the total number of fused rings (N) presented in Table 3.1 plus three

new ones H-SiNR(7,7), H-SiNR(8,8), and H-SiNR(9,9), and the results are shown in Fig. 3-6 . From Fig. 3-6, we note that the H-L energy gap decreases as N increases more for the singlet state than for the triplet state. A similar trend has been reported for carbon clusters with different diameters [39]. We can expect that for $N < 10$, quantum confinement effects become important, so a large energy gap may be expected. Additionally for $N < 10$, we observe that the ground state is simply given by the singlet state. The H-L energy gaps for the triplet state are lower in energy than for the singlet state, indicating that the H-SiNRs in the armchair direction shows lower band gaps since the triplet state is more stable for $n_a > n_z$. We can notice that for $N = 64$, the H-L gaps for the singlet and triplet state become almost degenerate. In the limit $N \to \infty$ or for finite temperature calculations (as previously indicated for room temperature graphene nanoribbons [40]), we would expect a dramatic reduction of the HL band gap of silicene to 0 eV, and its electronic properties could become similar to those of pure graphene such as a high mobile carrier density [73].

3.3 Conclusions

Using first-principles calculations, we showed that the singlet ground state of H-SiNRbs becomes multi-configurational upon increasing the size of the system, meaning that one determinant first principles methods may become inefficient for its description. Insight from the spin contamination provides good reason to believe that states with higher multiplicity may become relevant as the width of the ribbon increases. Depending on whether the ribbon edges are along armchair or zigzag directions, the ground state can be a singlet state (antiferromagnetic) for $n_z > n_a$, or a triplet state (ferromagnetic) for $n_a > n_z$. The calculated Raman spectra for the different multiplicities allows us to calculate a D peak which is given by the armchair edges with a triplet ground state. Additionally, we show that the H-L gap decreases for both the singlet and triplet states; however, in comparing the singlet and triplet cases containing the same number of Si and H atoms, the H-L gap decays faster for the singlet state. The decay of the H-L gap in the singlet case shows that the H-L gap dismin-

ishes for a very large N as expected. Therefore, we found that silicene itself could be a material with a zero band gap for a very large system as previously reported, while a finite system of silicene is expected to exhibit a non-zero H-L gap which depends on the number of fused rings N and the topology of their edges, i.e. armchair versus zigzag. Knowledge of the H-L gap and its tunability as a function of the nanoribbon length would make silicene a good candidate for nanotechnology applications.

Furthermore, the calculation of the Raman spectra was done to bridge theory with experiment, as well as a tool to identify the singlet and triplet states. What needs to be done now in order to provide more theoretical evidence for the preference of the triplet state when $n_a > n_z$, is to calculate either H-SiNR(4,7) or H-SiNR(4,8) energy using finite temperature dynamics at T $>$ 300K and observe if the triplet is still the ground state along with the closing of its H-L gap. Additionally, it is important to see how these systems couple with a metallic substrate now that current synthesis technics for low dimensional materials are usually done in this way. If latter observations are researched, possibly more experimentalists would be interested on taking up the endeavour of producing such nano-scaled systems.

Appendix A

Why B3LYP?

A commonly overlooked and unfortunate problem of dealing with DFT calculations is that not any functional yields reliable results for all types of systems, for example it has been demonstrated that GGA (PBE, PW91, etc.) and local density approximation (LDA) functionals frequently underestimate band gap energies of many semiconductors, the extent of the error could be as severe as obtaining a metallic state for well known insulators and semiconductors [78]. The latter is due to derivative discontinuities of the approximated exchange-correlation energy[57], by contrast, the Hartree-Fock (HF) approach overestimates band gap energies because of the increased localization of the electronic states brought on by including the exact exchange in its method. Hence, it has been reported that hybrid functionals in general provide more dependable and notably better band gap energies for most insulators and semiconductors [47], demonstrating a mean average deviation (MAD) of 0.19 eV for select semiconductors [78]. Additionally, in [58] various functionals were analyzed with respect to a material's H-L gap and its fundamental gap (the fundamental gap of a material is the energy difference between its conduction band and valence band) where once again hybrid functionals outperform the other by obtaining more accurate band gaps. Another reason of selecting B3LYP was obtained through comparison with M062x and PBE by calculating the geometrical optimization of disilane ($H_3Si-SiH_3$) and comparing their results, which are reported in table A.1. At first glance, they all more or less seem like great candidates, but because of the size of disilane, we have

Table A.1: Experimental and computed results for disilane (the cc-pVDZ base was used for all calculations).

Type	Experiment	B3LYP	M062x	PBE
$d_{\mathrm{Si-Si}}$[Å]	2.331[10]	2.358	2.348	2.357
$d_{\mathrm{Si-H}}$[Å]	1.492[10]	1.497	1.491	1.51
∠Si-Si-H	110.3°,[60]	110.3°	110.2°	110.3°
∠H-Si-H	108.6°,[60]	108.7°	108.8°	108.6°

not evaluated the dispersion effects around the Si-Si bond. Thus we substituted the hydrogens in the disilane molecule with mesityl (Mes) to obtain $Mes_2Si = SiMes_2$. According to the results reported in table A.2, the B3LYP functional provides us with the exact bonding distance as the experimental result. Consequently, B3LYP became our choice for all of the DFT calculations realized in this study of silicene nanoribbons, amid with previous arguments that hybrid functionals obtain more accurate gap energies. Finally, a recent article [41] has exposed a common flaw concerning most of the newer functionals since the year 2000, a trait essential for the obtention of the exact exchange-correlation functional, in which most have strayed from their ability of calculating accurate electron densities. This is because most newer functionals have focused on better energies and geometries through the parametrization of greater physical-chemical data sets which is what ultimately hurts their theoretical foundations necessary to predict correct electron densities. It is thus quite fortunate to see that overall, from an analysis spanning a total of 128 functionals, B3LYP was listed among the best functionals with overall performance; accurate for energetic, geometric and electron density calculations, all of which were used in the analysis of our systems.

Table A.2: Experimental and computed results for $Mes_2Si = SiMes_2$ (the cc-pVDZ base was used for all calculations).

Type	Experiment	B3LYP	M062x	PBE
$d_{\mathrm{Si-Si}}$[Å]	2.16[63]	2.16	2.148	2.19

Bibliography

[1] TURBOMOLE V7.1 2016, a development of University of Karlsruhe and Forschungszentrum Karlsruhe GmbH, 1989-2007, TURBOMOLE GmbH, since 2007; available from
`http://www.turbomole.com`.

[2] S. Cahangirov, M. Topsakal, E. Aktürk, H. Şahin, and S. Ciraci. Two- and one-dimensional honeycomb structures of silicon and germanium. *Phys. Rev. Lett.*, 102:236804, 2009.

[3] L. G. Cançado, M. A. Pimenta, B. R. A. Neves, M. S. S. Dantas, and A. Jorio. Influence of the atomic structure on the raman spectra of graphite edges. *Phys. Rev. Lett.*, 93:247401, Dec 2004.

[4] C. Casiraghi, A. Hartschuh, H. Qian, S. Piscanec, C. Georgi, A. Fasoli, K. S. Novoselov, D. M. Basko, and A. C Ferrari. Raman spectroscopy of graphene edges. *Nano Lett.*, 9:1433, 2009.

[5] Jian-Hao Chen, Chaun Jang, Shudong Xiao, Masa Ishigami, and Michael S. Fuhrer. Intrinsic and extrinsic performance limits of graphene devices on sio2. *Nat Nano*, 3(4):206–209, 04 2008.

[6] Manish Chhowalla, Debdeep Jena, and Hua Zhang. Two-dimensional semiconductors for transistors. *Nature Reviews Materials*, 1:16052, 08 2016.

[7] A. J. Cohen, D. J. Tozer, and N. C. J Handy. Evaluation of s2 in density functional theory. *J. Chem. Phys.*, 126:214104, 2007.

[8] P. A. M. Dirac. Note on exchange phenomena in the thomas atom. *Mathematical Proceedings of the Cambridge Philosophical Society*, 26(3):376–385, 007 1930.

[9] Editorial. Expanding our 2d vision. *Nature Reviews Materials*, 1:16089, 11 2016.

[10] Ernest L. Eliel and Samuel H. Wilen. *Stereochemistry of Organic Compounds*. Wiley, 1st edition, 1994.

[11] B. Feng, Z. Ding, S. Meng, Y. Yao, X. He, P. Cheng, L. Chen, and K. Wu. Evidence of silicene in honeycomb structures of silicon on ag(111). *Nano Lett.*, 12:3507, 2012.

[12] E. Fermi. Un metodo statistico per la determinazione di alcune priorieta dell'atomo. *Atti Acad.Naz.Lincei, Rend.*, 6:602–607, 1927.

[13] A. C. Ferrari, J. C. Meyer, V. Scardaci, C. Casiraghi, M. Lazzeri, F. Mauri, S. Piscanec, D. Jiang, K. S. Novoselov, S. Roth, and A. K Geim. Raman spectrum of graphene and graphene layers. *Phys. Rev. Lett.*, 97:187401, 2006.

[14] A. Fleurence, R. Friedlein, T. Ozaki, H. Kawai, Y. Wang, and Y. Yamada-Takamura. Experimental evidence for epitaxial silicene on diboride thin films. *Phys. Rev. Lett.*, 108:245501, 2012.

[15] M. J. Frisch, G. W. Trucks, H. B. Schlegel, G. E. Scuseria, M. A. Robb, J. R. Cheeseman, G. Scalmani, V. Barone, G. A. Petersson, H. Nakatsuji, X. Li, M. Caricato, A. V. Marenich, J. Bloino, B. G. Janesko, R. Gomperts, B. Mennucci, H. P. Hratchian, J. V. Ortiz, A. F. Izmaylov, J. L. Sonnenberg, D. Williams-Young, F. Ding, F. Lipparini, F. Egidi, J. Goings, B. Peng, A. Petrone, T. Henderson, D. Ranasinghe, V. G. Zakrzewski, J. Gao, N. Rega, G. Zheng, W. Liang, M. Hada, M. Ehara, K. Toyota, R. Fukuda, J. Hasegawa, M. Ishida, T. Nakajima, Y. Honda, O. Kitao, H. Nakai, T. Vreven, K. Throssell, J. A. Montgomery, Jr., J. E. Peralta, F. Ogliaro, M. J. Bearpark, J. J. Heyd, E. N. Brothers, K. N. Kudin, V. N. Staroverov, T. A. Keith, R. Kobayashi, J. Normand, K. Raghavachari, A. P. Rendell, J. C. Burant, S. S. Iyengar, J. Tomasi, M. Cossi, J. M. Millam, M. Klene, C. Adamo, R. Cammi, J. W. Ochterski, R. L. Martin, K. Morokuma, O. Farkas, J. B. Foresman, and D. J. Fox. Gaussian˜09 Revision D.01, 2013. Gaussian Inc. Wallingford CT.

[16] Mitsutaka Fujita, Katsunori Wakabayashi, Kyoko Nakada, and Koichi Kusakabe. Peculiar localized state at zigzag graphite edge. *Journal of the Physical Society of Japan*, 65(7):1920–1923, 1996.

[17] P. Ganesh, J. Kim, C. Park, M. Yoon, F. A. Reboredo, and P. R. C. Kent. Binding and diffusion of lithium in graphite: Quantum monte carlo benchmarks and validation of van der waals density functional methods. *J. Chem. Theory Comput.*, 10:5318, 2014.

[18] S. Grimme, J. Antony, S. Ehrlich, and H. Krieg. A consistent and accurate ab initio parametrization of density functional dispersion correction (dft-d) for the 94 elements h-pu. *J. Chem. Phys.*, 132:154104, 2010.

[19] Z. X. Guo, S. Furuya, J. I. Iwata, and A. Oshiyama. Absence and presence of dirac electrons in silicene on substrates. *Phys. Rev. B: Condens. Matter Mater. Phys.*, 87:235435, 2013.

[20] G. G. Guzmán-Verri and L. C. Lew Yan Voon. Electronic structure of silicon-based nanostructures. *Phys. Rev. B: Condens. Matter Mater. Phys.*, 76:075131, 2007.

[21] Fred A. Hamprecht, Aron J. Cohen, David J. Tozer, and Nicholas C. Handy. Development and assessment of new exchange-correlation functionals. *The Journal of Chemical Physics*, 109(15):6264–6271, 1998.

[22] P. Hohenberg and W. Kohn. Inhomogeneous electron gas. *Phys. Rev.*, 136:B864–B871, Nov 1964.

[23] M. Huzak, M. S. Deleuze, and B. Hajgató. Half-metallicity and spin-contamination of the electronic ground state of graphene nanoribbons and related systems: An impossible compromise? *J. Chem. Phys.*, 135:104704, 2011.

[24] Frank Jensen. *Introduction to Computational Chemistry*. John Wiley Sons, Ltd., 2nd edition, 2007.

[25] A. Kara, H. Enriquez, A. P. Seitsonen, L. C. Lew Yan Voon, S. Vizzini, B. Aufray, and H. Oughaddou. A review on silicene - new candidate for electronics. *Surf. Sci. Rep.*, 67:1, 2012.

[26] K. Kim and K. D. Jordan. Comparison of density functional and mp2 calculations on the water monomer and dimer. *The Journal of Physical Chemistry*, 98(40):10089–10094, 1994.

[27] P. J. Knowles and N. C Handy. Projected unrestricted mo/ller-plesset second-order energies. *J. Chem. Phys.*, 88:6991, 1988.

[28] Wolfram Koch and Max C. Holthausen. *A Chemist's Guide to Density Functional Theory*. Wiley-VCH Verlag GmbH, 2nd edition, 2001.

[29] W. Kohn and L. J. Sham. Self-consistent equations including exchange and correlation effects. *Phys. Rev.*, 140:A1133–A1138, Nov 1965.

[30] A. Köhler and D. Beljonne. The singlet–triplet exchange energy in conjugated polymers. *Adv. Funct. Mater.*, 14:11, 2004.

[31] L. D. Landau. Zur Theorie der phasenumwandlungen II. *Phys. Z. Sowjetunion*, 11:26–35, 1937.

[32] Chengteh Lee, Weitao Yang, and Robert G. Parr. Development of the colle-salvetti correlation-energy formula into a functional of the electron density. *Phys. Rev. B*, 37:785–789, Jan 1988.

[33] Hosik Lee, Young-Woo Son, Noejung Park, Seungwu Han, and Jaejun Yu. Magnetic ordering at the edges of graphitic fragments: Magnetic tail interactions between the edge-localized states. *Phys. Rev. B*, 72:174431, Nov 2005.

[34] Mel Levy. Universal variational functionals of electron densities, first-order density matrices, and natural spin-orbitals and solution of the v-representability problem. *Proceedings of the National Academy of Sciences*, 76(12):6062–6065, 1979.

[35] Elliott H. Lieb. Thomas-fermi and related theories of atoms and molecules. *Rev. Mod. Phys.*, 53:603–641, Oct 1981.

[36] J. Linder and J. W. A. Robinson. Superconducting spintronics. *Nat. Phys.*, 11:307, 2015.

[37] C. C. Liu, W. Feng, and Y. Yao. Quantum spin hall effect in silicene and two-dimensional germanium. *Phys. Rev. Lett.*, 107:076802, 2011.

[38] C. C. Liu, H. Jiang, and Y. Yao. Low-energy effective hamiltonian involving spin-orbit coupling in silicene and two-dimensional germanium and tin. *Phys. Rev. B: Condens. Matter Mater. Phys.*, 84:195430, 2011.

[39] M. Lonfat, B. Marsen, and K Sattler. The energy gap of carbon cluster studied by scanning tunneling spectroscopy. *Chem. Phys. Lett.*, 313:539, 1999.

[40] Gabor Zsolt Magda, Xiaozhan Jin, Imre Hagymasi, Peter Vancso, Zoltan Osvath, Peter Nemes-Incze, Chanyong Hwang, Laszlo P. Biro, and Levente Tapaszto. Room-temperature magnetic order on zigzag edges of narrow graphene nanoribbons. *Nature*, 514(7524):608–611, 10 2014.

[41] Michael G. Medvedev, Ivan S. Bushmarinov, Jianwei Sun, John P. Perdew, and Konstantin A. Lyssenko. Density functional theory is straying from the path toward the exact functional. *Science*, 355(6320):49–52, 2017.

[42] N. D. Mermin. Crystalline order in two dimensions. *Phys. Rev.*, 176:250–254, Dec 1968.

[43] Alessandro Molle, Carlo Grazianetti, Daniele Chiappe, Eugenio Cinquanta, Elena Cianci, Grazia Tallarida, and Marco Fanciulli. Hindering the oxidation of silicene with non-reactive encapsulation. *Advanced Functional Materials*, 23(35):4340–4344, 2013.

[44] G. E. Moore. Cramming more components onto integrated circuits, reprinted from electronics, volume 38, number 8, april 19, 1965, pp.114 ff. *IEEE Solid-State Circuits Society Newsletter*, 11(5):33–35, Sept 2006.

[45] G. E. Moore. Progress in digital integrated electronics [technical literaiture, copyright 1975 ieee. reprinted, with permission. technical digest. international electron devices meeting, ieee, 1975, pp. 11-13.]. *IEEE Solid-State Circuits Society Newsletter*, 20(3):36–37, Sept 2006.

[46] R. S. Muller and T. I. Kamins. *Device Electronics for Integrated Circuits*. John Wiley Sons, Ltd., 3rd edition, 2003.

[47] J. Muscat, A. Wander, and N. M Harrison. On the prediction of band gaps from hybrid functional theory. *Chem. Phys. Lett.*, 342:397, 2001.

[48] Kyoko Nakada, Mitsutaka Fujita, Gene Dresselhaus, and Mildred S. Dresselhaus. Edge state in graphene ribbons: Nanometer size effect and edge shape dependence. *Phys. Rev. B*, 54:17954–17961, Dec 1996.

[49] Z. Ni, Q. Liu, K. Tang, J. Zheng, J. Zhou, R. Qin, Z. Gao, D. Yu, and J. Lu. Tunable bandgap in silicene and germanene. *Nano Lett.*, 12:113, 2012.

[50] K. S. Novoselov, A. K. Geim, S. V. Morozov, D. Jiang, M. I. Katsnelson, I. V. Grigorieva, S. V. Dubonos, and A. A. Firsov. Two-dimensional gas of massless dirac fermions in graphene. *Nature*, 438(7065):197–200, 11 2005.

[51] K. S. Novoselov, A. K. Geim, S. V. Morozov, D. Jiang, Y. Zhang, S. V. Dubonos, I. V. Grigorieva, and A. A. Firsov. Electric field effect in atomically thin carbon films. *Science*, 306(5696):666–669, 2004.

[52] K. S. Novoselov, D. Jiang, F. Schedin, T. J. Booth, V. V. Khotkevich, S. V. Morozov, and A. K. Geim. Two-dimensional atomic crystals. *Proceedings of the National Academy of Sciences of the United States of America*, 102(30):10451–10453, 2005.

[53] Ricardo Pablo-Pedro, Hector Lopez-Rios, Serguei Fomine, and Mildred S. Dresselhaus. Detection of multiconfigurational states of hydrogen-passivated silicene nanoclusters. *The Journal of Physical Chemistry Letters*, 8(3):615–620, 2017. PMID: 28088863.

[54] Paola De Padova, Claudio Quaresima, Bruno Olivieri, Paolo Perfetti, and Guy Le Lay. sp2-like hybridization of silicon valence orbitals in silicene nanoribbons. *Applied Physics Letters*, 98(8):081909, 2011.

[55] R. Peierls. Quelques propriétés typiques des corps solides. *Annales de l'institut Henri Poincaré*, 5(3):177–222, 1935.

[56] John P. Perdew, Kieron Burke, and Matthias Ernzerhof. Generalized gradient approximation made simple. *Phys. Rev. Lett.*, 77:3865–3868, Oct 1996.

[57] John P. Perdew and Mel Levy. Physical content of the exact kohn-sham orbital energies: Band gaps and derivative discontinuities. *Phys. Rev. Lett.*, 51:1884–1887, Nov 1983.

[58] John P. Perdew, Weitao Yang, Kieron Burke, Zenghui Yang, Eberhard K. U. Gross, Matthias Scheffler, Gustavo E. Scuseria, Thomas M. Henderson, Igor Ying Zhang, Adrienn Ruzsinszky, Haowei Peng, Jianwei Sun, Egor Trushin, and Andreas Görling. Understanding band gaps of solids in generalized kohn–sham theory. *Proceedings of the National Academy of Sciences*, 114(11):2801–2806, 2017.

[59] M. A. Pimenta, G. Dresselhaus, M. S. Dresselhaus, L. G. Cançado, A. Jorio, and R. Saito. Studying disorder in graphite-based systems by raman spectroscopy. *Phys. Chem. Chem. Phys.*, 9:1276, 2007.

[60] Russell M. Pitzer. The barrier to internal rotation in ethane. *Accounts of Chemical Research*, 16(6):207–210, 1983.

[61] F. Plasser, H. Pašalić, M. H. Gerzabek, F. Libisch, R. Reiter, J. Burgdörfer, T. Müller, R. Shepard, and H. Lischka. The multiradical character of one- and two-dimensional graphene nanoribbons. *Angew. Chem., Int. Ed.*, 52:2581, 2013.

[62] R. Quhe, Y. Yuan, J. Zheng, Y. Wang, Z. Ni, J. Shi, D. Yu, J. Yang, and J. Lu. Does the dirac cone exist in silicene on metal substrates? *Sci. Rep.*, 4:1, 2014.

[63] Gerhard Raabe and Josef Michl. Multiple bonding to silicon. *Chemical Reviews*, 85(5):419–509, 1985.

[64] B. O. Roos, P. R. Taylor, and P. E. M. Siegbahn. A complete active space scf method (casscf) using a density matrix formulated super-ci approach. *Chem. Phys.*, 48:157, 1980.

[65] H. Sahaf, L. Masson, C. Léandri, B. Aufray, G. Le Lay, and F. Ronci. Formation of a one-dimensional grating at the molecular scale by self-assembly of straight silicon nanowires. *Applied Physics Letters*, 90(26):263110, 2007.

[66] John R. Schaibley, Hongyi Yu, Genevieve Clark, Pasqual Rivera, Jason S. Ross, Kyle L. Seyler, Wang Yao, and Xiaodong Xu. Valleytronics in 2d materials. *Nature Reviews Materials*, 1:16055, 08 2016.

[67] H. B. Schlegel. Potential energy curves using unrestricted mo/ller–plesset perturbation theory with spin annihilation. *J. Chem. Phys.*, 84:4530, 1986.

[68] Young-Woo Son, Marvin L. Cohen, and Steven G. Louie. Half-metallic graphene nanoribbons. *Nature*, 444(7117):347–349, 11 2006.

[69] C. D. Stanciu, A. V. Kimel, F. Hansteen, A. Tsukamoto, A. Itoh, A. Kirilyuk, and Th. Rasing. Ultrafast spin dynamics across compensation points in ferrimagnetic GdFeCo: The role of angular momentum compensation. *Phys. Rev. B*, 73:220402, Jun 2006.

[70] P. J. Stephens, F. J. Devlin, C. F. Chabalowski, and M. J. Frisch. Ab initio calculation of vibrational absorption and circular dichroism spectra using density functional force fields. *The Journal of Physical Chemistry*, 98(45):11623–11627, 1994.

[71] Attila Szabo and Neil S. Ostlund. *Modern Quantum Chemistry: Introduction to Advanced Electronic Structure Theory*. Dover Publications, INC., 1st revised edition, 1996.

[72] K. Takeda and K. Shiraishi. Theoretical possibility of stage corrugation in si and ge analogs of graphite. *Phys. Rev. B: Condens. Matter Mater. Phys.*, 50:14916, 1994.

[73] L. Tao, E. Cinquanta, D. Chiappe, C. Grazianetti, M. Fanciulli, M. Dubey, A. Molle, and D. Akinwande. Silicene field-effect transistors operating at room temperature. *Nat. Nanotechnol.*, 10:227, 2015.

[74] Li Tao, Eugenio Cinquanta, Daniele Chiappe, Carlo Grazianetti, Marco Fanciulli, Madan Dubey, Alessandro Molle, and Deji Akinwande. Silicene field-effect transistors operating at room temperature. *Nat Nano*, 10(3):227–231, 03 2015.

[75] L. H. Thomas. The calculation of atomic fields. *Mathematical Proceedings of the Cambridge Philosophical Society*, 23(5):542–548, 001 1927.

[76] Ana E. Torres, Patricia Guadarrama, and Serguei Fomine. Multiconfigurational character of the ground states of polycyclic aromatic hydrocarbons. a systematic study. *Journal of Molecular Modeling*, 20(5):2208, 2014.

[77] A. J. Williamson, R. Q. Hood, R. J. Needs, and G. Rajagopal. Diffusion quantum monte carlo calculations of the excited states of silicon. *Phys. Rev. B: Condens. Matter Mater. Phys.*, 57:12140, 1998.

[78] Hai Xiao, Jamil Tahir-Kheli, and William A. Goddard. Accurate band gaps for semiconductors from density functional theory. *The Journal of Physical Chemistry Letters*, 2(3):212–217, 2011.

[79] J. A. Yan, T. Stein, D. M. Schaefer, X. Q. Wang, and M. Y Chou. Electron-phonon coupling in two-dimensional silicene and germanene. *Phys. Rev. B: Condens. Matter Mater. Phys.*, 88:121403, 2013.

[80] X. Zhang, H. Xie, M. Hu, H. Bao, S. Yue, G. Qin, and G. Su. Thermal conductivity of silicene calculated using an optimized stillinger-weber potential. *Phys. Rev. B: Condens. Matter Mater. Phys.*, 89:054310, 2014.

[81] J. Zhuang, X. Xu, Y. Du, K. Wu, L. Chen, W. Hao, J. Wang, W. K. Yeoh, X. Wang, and S. X Dou. Investigation of electron-phonon coupling in epitaxial silicene by in situ raman spectroscopy. *Phys. Rev. B: Condens. Matter Mater. Phys.*, 91:161409, 2015.